STRENGTH OF SPOT WELDING OF AISI316 METAL SHEETS FOR MEDICAL USE

Mohamed Balaid A RMADAN

2021
MASTER THESIS
MECHANICAL ENGINEERING

Thesis Advisor
Assoc.Prof.Dr. Ismail ESEN

STRENGTH OF SPOT WELDING OF AISI316 METAL SHEETS FOR MEDICAL USE

Mohamed Balaid A RMADAN

T.C.
Karabuk University
Institute of Graduate Programs
Department of Mechanical Engineering
Prepared as
Master Thesis

Thesis Advisor
Assoc.Prof.Dr. Ismail ESEN

KARABUK
July 2021

I certify that in my opinion the thesis submitted by Mohamed Balaid A RMADAN titled "STRENGTH OF SPOT WELDING OF AISI 316 METAL SHEETS FOR MEDICAL USE " is fully adequate in scope and in quality as a thesis for the degree of Master of Science.

Assoc.Prof.Dr. Ismail ESEN .....
Thesis Advisor, Department of Mechanical Engineering

This thesis is accepted by the examining committee with a unanimous vote in the Department of Mechanical Engineering as a Master of Science thesis. July 16, 2021

Examining Committee Members (Institutions)	Signature
Chairman : Assoc.Prof.Dr. Ismail ESEN (KBU)	.....
Member : Assoc.Prof.Dr. Selami SAGIROGLU (KBU)	.....
Member : Assist.Dr. Mehmet Akif KOC (SAU)	.....

The degree of Master of Science by the thesis submitted is approved by the Administrative Board of the Institute of Graduate Programs, Karabuk University.

Prof. Dr. Hasan SOLMAZ .....
Director of the Institute of Graduate Programs

"I declare that all the information within this thesis has been gathered and presented in accordance with academic regulations and ethical principles and I have according to the requirements of these regulations and principles cited all those which do not originate in this work as well."

Mohamed Balaid A RMADAN

ABSTRACT

M. Sc. Thesis

STRENGTH OF SPOT WELDING OF AISI316 METAL SHEETS FOR MEDICAL USE

Mohamed Balaid A RMADAN

Karabük University
Institute of Graduate Programs
The Department of Mechanical Engineering

Thesis Advisor:
Assoc. Prof. Dr. Ismail ESEN
July 2021, 88 pages

Stainless steel (SS), chromium (Cr) alloys, titanium (Ti) and Ti alloys are unique metallic biomaterials used for implant materials. The use of SS as medical material has become an important area due to its capacity to increase longevity and quality of life. Although AISI 316L metal sheets used for medical purposes have a wide application area, studies on them are limited in our country. In this study, the application areas, mechanical and metallurgical properties of general strength spot welding of AISI 316 sheets for medical uses were investigated. This research study identified some material constants such as resistance spot welding (RSW) of AISI 316 metal sheets for medical uses.

Key Words : AISI 316L, stainless steel, resistance welding, tensile test, strength of resistance spot welding

Science Code : 91415

ÖZET

Yüksek Lisans Tezi

TIBBI ALANLARDA KULLANILAN AISI316 METAL SACLARIN DİRENÇ NOKTA KAYNAĞI DAYANIMI

Mohamed Balaid A RMADAN

Karabük Üniversitesi
Lisansüstü Eğitim Enstitüsü
Makine Mühendisliği Anabilim Dalı

Tez Danışmanı:
Doç. Dr. İsmail Esen
Temmuz 2021, 88 sayfa

Paslanmaz çelikler, kobalt-krom alaşımları, ticari olarak saf titanyum ve alaşımları, implant malzemeleri için kullanılan tipik metalik biyomalzemelerdir. Paslanmaz çeliklerin tıbbi malzeme olarak kullanımı insan yaşamının kalitesini ve ömrünü artırabilme kapasitesinden dolayı önemli bir alan haline gelmiştir. Tıbbi amaçla kullanılan AISI 316 metal levhalar geniş bir uygulama alanına sahip olmasına rağmen ülkemizde bunlarla ilgili çalışmalar sınırlıdır. Bu çalışmada, AISI 316 sacların genel mukavemetli punta kaynağının tıbbi kullanımlar için uygulama alanları, mekanik ve metalurjik özellikleri araştırılmıştır. Bu araştırma çalışması, tıbbi kullanımlar için AISI 316 metal levhaların mukavemet nokta kaynağı gibi bazı malzeme sabitlerini tanımlamıştır.

Anahtar Kelimeler : AISI 316L, paslanmaz çelik, direnç nokta kaynağı, çekme testi, direnç nokta kaynağının dayanımı

Bilim Kodu : 91415

ACKNOWLEDGMENT

First of all, I would like to give thanks to my advisor, Assoc. Prof. Dr. Ismail ESEN, for his great interest and assistance in preparation of this thesis.

CONTENTS

Page

Page

Page

LIST OF FIGURES

Page

Page

LIST OF TABLES

Page

SYMBOLS AND ABBREVITIONS INDEX

ABBREVITIONS

SS	: Stainless Steels
CoR	: Corrosion Resistance
FS	: Ferritic (Stainless) Steels
MS	: Martensitic (Stainless) Steels
AS	: Austenitic (Stainless) Steels
DS	: Duplex (Stainless) Steels
PHS	: Precipitation-Hardening (Stainless) Steels
RSW	: Resistance Spot Welding
FP	: Ferrit Phase
AP	: Austenit Phase
MP	: Martensit Phase
BCC	: Body Centered Cubic
FCC	: Face Centered Cubic
Ni	: Nickel
Cr	: Chromium
Ti	: Titanium
O	: Oxygen
Mo	: Molybdenum
C	: Carbon
Fe	: Iron
Co	: Cobalt
AISI	: American Iron and Steel Institute
SAF	: Sandvik Austenite Ferrite

PART 1

INTRODUCTION

In the health industry, metallic materials are widely preferred in order to repair or increase the functionality of the tissues of the human body that have lost their function or are damaged. As a result of the widespread use of metallic or some structural materials in body structures, they have been named biomaterials due to their high biocompatibility. Biomaterials consist of natural or artificial materials that are used to restore damaged, dysfunctional or diseased biological structure and restore functionality. In general, biomaterials help improve people's quality of life and their longevity. Today, the field of biomaterials has grown more than expected to meet the aging population demands of countries. Biomaterials are often used in different parts of the human body. Artificial valves in the heart, Blood vessels stents, shoulders implants, and knee, hip, elbow, and tooth structures are examples of this [1].

Implants are generally used by being fixed to the skeletal system of the human body to aid healing, repair damaged areas and restore lost functions in body tissues. Especially orthopedic implants have managed to improve the quality of life of millions of people in the last 25-30 years.

The most important issue in orthopedic implants is corrosion resistance (CoR). The CoR of these materials is related to the presence of the oxide film on their surface. Even though the CoR of the oxide film is relatively high in most SS groups, the oxide film is highly susceptible to different forms of corrosion pitting, splitting and stress-induced cracking. However, austenitic SS, and especially AISI 316L, are widely used as orthopedic implants due to their many advantages such as good mechanical properties, low cost, good CoR, wider usability and easy processing [1].

Today, materials used in biomaterials, in particular for load-bearing practices, must have an excellent combination of high strength and superior CoR in the body environment, high fatigue, and ductility, wear-resistance, and should not have cytotoxicity. Therefore, the materials used in orthopedics in accordance with these properties are ceramics, polymers, metals and alloys, and composites.

Metallic materials are more preferred as biomaterials due to their higher tensile strength, high fatigue strength and high fracture toughness compared to polymeric and ceramic materials. Due to the ductility of metals, high strength and high yield points, it makes the properties of biomaterials suitable for load-bearing, which will be used in large deformations without permanent dimensional changes [1]. For this reason, SS biomaterials are applied in medical tools like external fixators, artificial joints, bone plates, screws, intramedullary nails, spinal fixations, spinal spacers, pacemaker sheaths, artificial heart valves, wires, stents, and dental implants [2].

The SS and SS alloys are absolutely important in medical like they play a very dominant role in fulfilling nearly every difficult factor that arises in implant applications [1]. Although AISI 316L SS, Cr alloys, Ti and Ti6Al4V alloys were originally developed for industrial purposes, these materials are for biomaterial uses due to their relatively high CoR and excellent mechanical properties have been tried [2].

The main criterion in election of any implant material is its good biocompatibility. Metals and alloys have been widely used in various forms as biomaterials after they were seen to ensure the required mechanical strength and plausible CoR with good biological compatibility. Today, AISI 316L, Cr alloys, Ti and Ti6Al4V alloys are frequently preferred SS biomaterials for implant tools [3]. These materials are adopted to the body environment due to the oxide film formed on their surfaces. Austenitic SS are the commonly applied material for medical applications. SS are easier to manufacture and weld crosschecked to Cr alloys, Ti, and Ti alloys. SS implants are applied like temporary implants to aid bone healing as well as fixed implants such as artificial joints [1].

The CoR of steel grows up with increasing Cr content. CoR steels are produced by adding more than 11% Cr, resulting in the formation of a fine, chemically resolute, and oxide film. An oxide film creates and remedies itself in the presence of oxygen (O). Steels containing more than 11% Cr are called SS.

According to their microstructure, SS is divided into three main categories: ferritic stainless steels (FS), martensitic stainless steels (MS), and austenitic stainless steels (AS). Amongst the three categories are just FS that does not contain nickel (Ni). On the other hand, FS is of poor quality to other SS in strength, toughness, machinability, weldability, and CoR. Also, a critical prerequisite for medical materials is the complete absence of ferromagnetism. That is why, in numerous respects FS are inadequate and unsuitable candidates for medical materials, as the microstructure of SS medical materials must be fully austenitic [2].

1.1. ABOUT THE STUDY

The field of biomaterials has become an important field due to the capacity of these materials to improve people's quality of life their longevity. SS materials are commonly used as biomaterials to modify the structural components of the human body. AS are more widely used as biomaterials due to their very low cost, good mechanical, CoR properties, and high biological compatibility compared to other SS materials. Although AISI 316L material, which is austenitic stainless steel and widely used for medical purposes, has a wide application area, studies on them are limited in our country.

In this study, general mechanical properties of AISI 316L sheets were investigated for uses after RSW applied with different currents and different times. In addition, in this experimental study, tensile tests were applied to determine the mechanical properties of AISI 316L, and chemical composition analysis was performed with a metal analysis spectrometer to determine the chemical properties. After the researches, the data obtained were compared with each other and many mechanical results were determined.

PART 2

LITERATURE REVIEW

Marashi and his team used RSW to join the AS and galvanized low carbon (C) steel. They examined the relationship between the failure mode and the size and microstructure in the source fusion region. They found that the RSW strength in the tensile failure mode is controlled by the strength of the galvanized steel side and the size of the melt zone. They deduced that the hardness of the fusion zone, dominated by the dilution among the two base metals, and the fusion zone size of the galvanized carbon steel side are the dominant factors in determining the failure mode [4].

A. B. Verma and his team investigated RSW properties in AISI 304, and AISI 316. In their study, tensile strength and hardness properties using Taguchi approach and ANOVA; using the Schaeffer diagram, they examined the microstructure of the ski area. In addition, attempts were made to link the quality of a weld to its qualities under the tensile-shear test and the effect of weld parameters on the weld metal size was evaluated. A. B. Verma and his team have reached many conclusions as a result of their work. Some of these results are as follows. First, they concluded that the tensile shear strength for different grades of AS (AISI 304 to AISI 316) is relatively higher compared to similar sheets (AISI 304 to AISI 304 / AISI 316 to AISI 316). Secondly, for the different RSW between the AS, an asymmetrical fusion zone was obtained due to the different electrical resistivity and thermal expansion coefficients. Finally, they concluded that although the hardness of the welded zone is higher than the hardness of the non-welded zone in AISI 304 and AISI 316 joints, there is a marginal increase in hardness in different joints [5].

Kamal Shelly and D. S. Sahota conducted a study on RSW applied on AISI 316 steel in their study. As a result of the study, they observed that the welding current is the main governing factor affecting the tensile shear strength of the RSW samples and the size of the weld zone increases as the welding current increases. They concluded that this increase would result in increased values of tensile-shear strength [6].

Haetham G. Mohammed et al. investigated the mechanical and microstructural properties of 3 mm thick RSW of AISI 316L. The reason for doing this study is the lack of findings in previous studies involving the use of 3 mm thick plates. They found that most of the studies focused on RSW of 316L with thickness below 2 mm. In this study, they investigated the effect of constant weld parameters on weld properties such as weld piece size, tensile-shear load of welded materials, micro-hardness, failure modes and microstructure of weld pieces. As a result of the study, they saw that the maximum tensile shear load was 21.549 kN. They concluded that the micro-hardness of the Fusion Zone is 230 HV, higher than the Base Metal (198.8 HV) and the Heat Effect Zone (HAZ) (184 HV), respectively [7].

T. Khuenkaew and K. Kanlayasiri sought to specify the ideal welding conditions for RSW in case of AISI 316 AS and AISI 425 FS, which present a challenge to differ. In their study, they examined several welding variables, including welding current, welding time, holding time and electrode strength, and top and bottom electrode types. At first, they used a $2^{(6-1)}$ fractional factorial to screen for the variables confused. Next, they used the Box-Behnken design to identify applicable multiple response optimizations to the size of the resource nuggets through the agency of analysis of these variables and the desirability function examination. The experiments were carried out using a RSW machine at 50 kVA, 50 Hz. The quality of welded samples was determined by penetration, nuggets diameter, and nuggets area. They concluded that the optimum welding conditions are 3.3 kN electrode force, 25 cycles of welding time, 10.000 amps of welding current, 50 cycles of holding time, and both R30 type up-low electrodes [8].

S. Fukumoto et al. have worked on small-scale RSW for AS. They obtained a welding lobe showing the process for making solid joints for AISI 304 SS thin sheets and

investigated the impacts of welding current and strength, and welding time on joint strength and nuggets size. They concluded that the cooling rate estimated from the solidification cell size in the study was almost 2.4x105 K/s, which is approximately similar to that produced by beam laser welding. They observed that the microstructure of the weld zones is approximately all austenitic due to the fast solidification rate. At the end of the study, they stated that despite the fully austenitic micro-structure, there was no hot cracking in the AS types AISI 302, 304, 316L, 310S, and 347 by RSW [9].

M. Pouranvari et al. conducted a two-stage study examining the effects of RSW on SS. In this two-part study, they aimed to understand the metallurgical phenomenon during RSW of SS. In the first chapter, the phase transformations of three types of SS in the fusion zone, including AS, FS, and duplex stainless steels (DS), are discussed. Hardening and solid-state with the inclusion of pillared to equiaxed transition, ferrite-austenite post-solidification transformation, martensitic transformation, and carbide precipitation are discussed. The impact of the high cooling rate of RSW on ferrite-austenite conversion was investigated. As a result, they completed the first part of their study by emphasizing the main factors controlling the stiffness of the fusion zone [10]. In the second part of the study, phase transformations in the heat-affected zone of three types of SS, including AS, FS, and DS are discussed. The failure modes and mechanical properties of RSW in SS are discussed. They concluded the second part of the study by comparing the peak load and energy absorption of RSW in SS with advanced high-strength steels [11].

Moshayedi and Sattari-Far performed numerical and experimental studies of nugget size growth in RSW of AS. In the study, a 2D axisymmetric electro-thermo-mechanical finite element model was developed to examine the effect of welding time and current density on nugget size in RSW of AISI 304L AS sheets using ANSYS commercial software package. In order to increase the accuracy, the temperature-dependent properties of the materials were taken into account during the simulation. The diameter and thickness of the calculated weld nuggets were compared with the experimental results. The finite element estimates of weld nugget growth and nugget size were in good agreement with the experimental results. The effects of welding time and current density on nugget growth were also investigated. As a result, they observed

that increasing welding time and current was accompanied by an increase in fusion zone size with decreasing slope. However, they noted that if ejection occurs, the size of the nugget will be reduced due to melting spatter. They concluded that weld time had little effect on nugget size compared to welding current, except for the initial nugget formation stage [12].

J. B. Shamsul et al. performed RSW on AISI 304 AS. In their study, they investigated the relationship between nugget diameter and welding current by welding AS type AISI 304 with RSW. They also studied the hardness distribution throughout the weld zone. As a result, they concluded that increasing welding current gives larger nugget diameter and welding current does not affect the hardness distribution much [13].

S. H. Arabi et al. investigated the impact of in situ control of thermal cycling during RSW as a tool for weld microstructure modification and improving the phase balance in the fusion zone of RSW of 2304 DS. Two different transformation paths were used to improve the phase balance in the fusion zone of SAF 2304 DS during RSW. The first of these is the downward gradient current modification, which aims to control the weld cooling rate. The second is the short annealing of the weld, which aims to form secondary austenite in the post-weld in situ fusion zone. It was determined that both ways allowed to increase the austenite volume fraction in the fusion zone. When they compared their methods with each other, they concluded that in situ post-weld annealing was more effective than downslope current modification. As a result of the inferences, they proved that creating a homogeneous microstructure with an improved phase balance through appropriate post-weld annealing can increase the CoR of the weld nugget when compared to the unstable fusion zone produced in the welded condition [14].

A. Moteshakker et al. studied the hardness and tensile properties of different weld joints among them SAF 2205 DS and AISI 316L. In the study, the mechanical properties of different weld joints among SAF 2205 DS and AISI 316L were investigated. They performed the welding process using different welding wires (AWS ER 347, AWS ER 316L, and AWS ER 309L). Micro-hardness and tensile tests were carried out in order to evaluate the hardness of the weld metal towards each side of the

metals and to determine the weld joints' strength. As a result of the processes, they observed that the weld metals of all samples exhibited higher hardness values than AISI 316L SS and lower values than SAF 2205 SS. They concluded that welding wire 309L exhibited higher mechanical properties, while welding wire 347 showed poor mechanical properties. According to the results, it was determined that 309L welding wire is suitable for welding duplex stainless steel to austenitic stainless steel by gas tungsten arc welding process [15].

U. Esme conducted a research on the optimization and effect of welding parameters on the tensile strength of spot welded SAE 1010 steel sheets. Experimental studies were carried out under varying electrode forces, welding currents, electrode diameters and welding times. Analysis of variance (ANOVA) was used to determine the importance of weld parameters on tensile shear strength. As a result of his validation tests, he concluded that it is possible to significantly increase the tensile strength by using the Taguchi method. As a result of the experiments, the validity of the Taguchi method used to improve the welding performance and optimize the welding parameters in the RSW process has been confirmed [16].

A. Bekmurzayeva and his team investigated the SS surface modification for biomedical applications. They stated that the existing literature on this subject is extensive and concluded that there is a deficiency in the literature because it was not addressed in an integrated way in previous reviews. In their study, they aimed to fill this lack of literature by examining the literature on surface modification methods of SS as well as the modification ways adapted for biomedical applications. As a result of their research, they have deduced that in many ongoing studies, they aim to overcome the inherent defects of SS and to meet new application needs with surface modification techniques. Comparing the methods reported in the literature, they concluded that surface treatment methods can result in improved performance of SS by simultaneously changing several surface properties important for biomedical applications [17].

Montasser M. Dewidar et al. studied the machining and mechanical properties of porous AISI 316L SS for biomedical applications. The AISI 316L SS parts were

fabricated using a powder metallurgy process that included selective laser sintering (SLS) and conventional sintering. In their study, they were able to produce AISI 316L suitable for medical applications, by controlling the SLS parameters and sintering behavior, with a volume ratio of 40-50% porosity. In addition, the study also investigates the porosity of sintered compact parts as a function of SLS parameters and furnace cycle. In the experimental study, the compressive stress and elastic modulus of AISI 316L SS material were determined and they found that the compressive strength was in the range of 21 to 32 MPa and the corresponding elastic modulus was in the range of 26 to 43 GPa. They have stated existing parts are promising for biomedical applications since the optimal porosity of implant materials for the growth of new bone tissues is in the range of 20% to 59% and the mechanical properties are compatible with human bone [18].

Bandar AL-Mangour et al. carried out a study on improving the strength and CoR of AISI 316L SS for biomedical applications using cold spray. They cold sprayed AISI 316L SS mixed with CoCr alloy L605 powders onto mild steel substrate. Since CoCr alone is difficult to spray, three different ratios (25%, 33.3% and 50% by CoCr volume) were cold sprayed. Analysis and characterization of the blasted deposits were carried out by scanning electron microscopy at room temperature, electron backscatter diffraction, micro-hardness and tensile tests. As a result of the spraying processes, they observed that the porosity of the surface coating was low for both 25% and 33.3% coating. However, they observed that the 50% coating had a much weaker settling rate and the porosity was much higher (about 4.5%), resulting in a much thinner coating using the same coating parameters. Corrosion behavior was evaluated using potentiodynamic polarization tests performed as electrolyte in Hank's solution. They found that the CoR of the metal-metal mixture is higher than that of pure SS [19].

Chun-Che Shih et al. investigated the effect of surface oxide properties on the CoR of AISI 316L for biomedical applications. In their study, they investigated the impact of different passive processes on the in vitro CoR of AISI 316L SS wire. In their work, characterization techniques such as anodic polarization testing, scanning electron microscopy, auger electron spectroscopy, X-ray photoelectron spectroscopy and transmission electron microscopy have been used to correlate corrosion behavior with

various surface properties and surface treatments. As a result of their study, they concluded that all these surface treatments did not satisfactorily improve the CoR of the alloy, except for amorphous oxidation. From the results, they deduced that the plastically deformed natural air-formed oxide layer had to be removed and could result from replacing a new enlarged, smoother and compact layer, which should consist of nanoscale oxide particles with higher O and Cr concentrations [20].

A. Amanov et al. studied low friction AISI 316L SS pipes for biomedical applications. In their work, they studied a non-destructive ultrasonic nanocrystalline surface modification (UNSM) to increase the strength of the AISI 316L SS pipe and improve its tribological performance. The UNSM-treated nanohardness and untreated nanohardness samples were evaluated using nanoindentation. They state that as a result of the study, a significant hardness increase was obtained for the UNSM-treated sample, which can be ascribed to nanocrystallization and refined grains. The untreated and UNSM-treated specimens' stress-strain behavior were evaluated with 3-point bending test. They discovered that the UNSM-treated sample exhibited higher strength than the untreated sample. They also indicate that the coefficient of friction and wear of the UNSM-treated resistance sample has significantly improved matched to the untreated sample. In the study, they concluded that there was a significant increase in hardness after the UNSM treatment and was due to the improved friction coefficient and pipe wear resistance. Therefore, experimental studies have found that the UNSM technique is beneficial in improving the mechanical and tribological properties of AISI 316L SS tubing for various medical applications, particularly coronary artery stents [21].

S. E. Barros et al. carried out a study on the mechanical strength of SS and Ti alloy mini-implants of different diameters. The lack of studies on the mechanical properties of SS mini-implants and Ti alloy mini-implants has led to a study on this subject. In the study, they tested the null hypothesis of no difference in the mechanical strength of SS mini-implants and Ti alloy mini-implants and analyzed tooth resistance to morphological damage after insertion of SS mini-implants and Ti alloy mini-implants. As a result of the study, they concluded that stainless steel mini-implants were 13.2% and 20.2% more resistant to torsional fracture and bending, respectively [22].

D.Amalraju and A.K.Shaik Dawood studied the mechanical strength evaluation analysis of SS and Ti locking plate for femur bone fracture. In their study, the stresses created by Ti6Al4V and AISI 316L SS materials in Femur Distal Locked Plate Implant under static load were analyzed using ANSYS software. Since each femur carries body weights half, they determined the load conditions by determining the excess weights, that is, the least possible weight and the heaviest possible weight. As a result of the analysis, they concluded that the loads had no effect on the failure of the implant, as they found the stress and deformation values to be very negligible. Also, they concluded that TI-6AL4V is a low-density material with excellent biocompatibility and mechanical properties, making it ideal for implant use in surgeries [23].

Douglas C. Hansen conducted a study on metal corrosion in the human body. In his study, he examined SS such as AISI 316L, CoCr alloys, Ti, nitinol. As a result of the reviews, he mentions that the greatest clinical improvements will be made with better material selection, design and quality control to reduce or possibly eliminate corrosion in medical devices. Surface modification of AISI 316L indicates that it is an alternative currently in practice. The study concluded that there are real risks associated with using metals other than AISI 316L SS as long-term chronic implant devices, and it has become clear that these risks can be managed and someday eliminated through continued research and development of new biomaterials [24].

V. Geanta et al. studied on SS with biological compatible properties for medical devices. In the study, AS (X5CrNi1810 / X5CrNiMo17122) and MS (X20CrMo13 / X35CrMo17) used in medical devices were emphasized. In experimental studies, they aimed to obtain austenitic and martensitic SS in vacuum arc remelting device and to examine the characterization of the obtained samples in terms of micro-structure and micro-hardness. In their experimental study, it is reported that the charge dosage was calculated correctly and the alloying order was well determined. Through the agency ofthe correct execution of the machining route, they achieved the desired steel composition gap. As a result of the study, they reached the conclusion that the average shrinkage, which was calculated as the ratio between the mass average value of the nugget and the load-mass average value, was over 99% [25].

D. Kianersi et al. studied the phase transformations, mechanical properties, and microstructure characterizations of AISI 316L sheets by making RSW joints. In their study, they aimed to optimize welding parameters such as welding current and time in RSW of AISI 316L quality sheets. In addition, the effects of optimum welding parameters on the RSW properties, and microstructure of AISI 316L sheets were investigated. A number of investigations were also carried out on welding properties such as the impact of welding current at constant welding time, weld nugget size, the load-carrying capacity of welded materials, the tensile-shear, failure modes, failure energy, ductility, and microstructure of weld nuggets. In the experimental studies, the phase transformations occurring during the welding thermal cycle were analyzed in detail, with the inclusion of the metallographic studies of the welding of AS, and data were collected. The metallographic images, mechanical properties, electron microscope photographs and micro-hardness measurements obtained from their experimental studies have concluded that the region between the transition from the interface to the tensile mode and the removal limit is described as the optimum welding condition. At the end of the study, they concluded that backscattered electron scanning microscopic images showed various delta ferrite types in the weld nuggets [26].

In another study, D. Kianersi and his team investigated the effects of welding current and time on the microstructure, mechanical characterization, and fractures of RSW joints of AISI 316L. In his studies, the impact of welding current and welding time on welding properties with the inclusion of weld nugget diameter or fusion zone, the tensile-shear, failure modes, the welded materials load-carrying capacity, energy absorption, and microstructure of welded nuggets have been tried to be discussed in detail. Experimental microstructural studies and obtained mechanical properties indicate that the region among the transition from the interface to the tensile mode and the extraction boundary is described qua the optimum welding condition. In the experimental studies, optimum microstructure and mechanical properties were obtained with the maximum tensile shear and load-carrying capacity or the welded materials peak load at 8070 N, with 8 kA welding current and 4 cycle welding time, and the failure mode is the button pull with tearing from the base metal have stated that it has occurred. At the end of the study, fracture surface studies concluded that

elongated pits were formed on the surface as a result of ductile fracture in the welded sample under optimum welding conditions [27].

M. S. M. Mansor et al. conducted a study investigating the microstructure and mechanical properties of micro-RSW between AISI 316L and Ti6Al4V. In their study, AISI 316L and Ti alloy (ASTM grade 5) materials were welded together by micro-RSW using a specially designed electrode geometry and in different combinations of welding parameters. Welded joints were submitted to the tensile shear strength test to determine the welded areas strength. In addition, microhardness and microstructural investigations (failure analysis) of the fracture mode were carried out to examine the effect of welding parameters on the welded joints during the welding process. At the end of the study, using the combination of 2.0 kN welding current, 100 ms welding time, and 241 N welding force, the highest load value obtained using the full factorial experimental design was determined as 378.25 N. The source current obtained in the study is the important parameter obtained by analysis of variance (ANOVA). However, they deduced that the increase in welding current must be controlled to prevent the weld metal from being ejected [28].

M. Vigneskumar et al. performed finite element-based parametric studies of RSW nugget diameter and temperature distribution of AISI 304 and AISI 316L. In their study, they investigated the RSW process of different AS sheets (AISI 304 / 316L) by varying the process parameters such as welding current and welding time at three different levels. Tensile shear tests and macrostructural studies were performed to analyze the point welds' performance. A three-dimensional model was also advanced using the commercial software ABAQUS FEA to predict the nugget diameter and thermal distribution profile through simultaneous structural electrothermal analysis with temperature-dependent material properties. The produced model was confirmed by comparing the estimated nugget diameter with the experimental nugget diameter. At the end of the experiments, the results showed good agreement with the simulation results and they concluded that the macrostructure of the point welded joints, the faultless fusion zone, and the successful welding of the different plates [29].

PART 3

STAINLESS STEELS

The earliest examples of SS were investigated in 1907 by Harry Brearley, who was in charge of the Brown-Firth Research Laboratory in Sheffield, England, looking for ways to get rid of rust buildup in the gun barrel. The first SS were discovered when he realized that a sample was not rusted among the rusty samples remaining from the tests he had done before, and he learned that the steel sample he had analyzed had a high content of Cr. Trying to find a steel that is more resistant to wear and effects, Brearley examined the grain structure of the steel by exposing the samples to many acids such as vinegar and lemon before examining them with a microscope. The etching samples he used saw that it was based on nitric acid and that this new type of steel strongly resisted chemical attack, and named these new CoR materials as SS. After this discovery of Harry Brearley, stainless steel production started rapidly in Europe. V2A steel, which was later developed by Krupp, is known as the first patented SS [30].

At the present time, there are close to 170 types of SS. These types of steel are widely used in many separate industrial areas. It is seen that the Cr ratio reaches up to 30% in different types of SS used in different industrial areas. In addition, thanks to the different elements added to SS, different properties such as machinability can be obtained [30].

The production of SS which is widely used in the industry is constantly developing with the development of technology and requires specialist skills. The preferred method in the melting and refining processes of SS is mostly the electric arc furnace/argon O decarbonization method. Thanks to this method, which was developed with the technology of the 1970s and applied by 80% of SS production, a significant decrease in production costs were achieved and at the same time, product

same time, product production is ensured without sacrificing quality. These advantages in SS production have led to the widespread use of the electric arc furnace/argon O decarbonization method.

The growth rate of SS production in today's industry has outstripped the growth rate of other metals and alloys. SS is one of the two most preferred metal materials along with aluminum (Al) alloys in the past 15 years. SS production in the world in 2007 was more than 29 000 000 tons, and SS productions have almost doubled in the previous decade. This increasing rate happened at the same time that stainless steel production continues to be further consolidated [31].

There is no doubt that SS are an important alloy class. Their importance is manifested in the multitude of applications based on their use. From the lowest quality such as cookware and furniture to the most complex and demanding applications such as aircraft and spacecraft, the use of SS is indispensable. Therefore, this functionality of SS, the ubiquity of SS in our daily life makes it impossible to count their applications [32].

While the word 'steel' means that most of the material is made up of the element iron (Fe), the use of the adjective 'stainless' indicates properties that indicate no staining, rusting, or corrosion in environments to which normal steels are susceptible. In order to make steels rustproof, Cr should be added at a rate of at least 11% by weight. This level of Cr allows for the formation of an adherent, self-healing Cr oxide on the steel surface in relatively benign environments. However, higher Cr contents must be added to protect against pitting and corrosion in the presence of elements such as O or C in more hostile environments [33].

While the Fe-Cr compound system forms the SS materials basis, modern SS contains outside of Cr several other alloying elements whose presence enhances certain properties. For example, molybdenum (Mo) is added to increase resistance to pitting, and Ni is added to obtain austenite. It is not unusual for some SS grades, such as super ferritic or super austenitic, to contain large amounts of these alloying elements. When the Cr and Ni element contents are added in significant amounts, the alloy that results

is called heat resistant alloys. Although there is a complex alloying element in SS, the total content of added elements is usually kept below the Fe element content level to ensure that the resulting alloy is steel. Metallurgical properties of SS are an element that should be well understood since changes can occur in their chemical structures according to their usage areas [33].

3.1. METALLURGY OF STAINLESS STEELS

Alloy systems, which are widely used in industry like C steels, C alloy steels, and Al alloys, are a number of elements diluted solutions in the main matrix of atomic structure. With some exceptions, C and C alloy steels consist of a magnetic body-centered cubic (BCC) phase or a different version of that with a slightly modified atomic cell structure. Al alloys share the face-centered cubic (FCC) atom cell structure of pure Al. It should be noted that in solid metals there may be several phases coexisting at the same time. The atomic cell structures of SS are an exceptional alloy system as it isn't a dilute solution. It is possible that alloy steels contain a few percent of alloying elements like C, Mn, Ni, Mo, Cr, and Si elements, intercalary to impurities of the elements sulfur, O, and phosphorus. In general, SS alloys include structurally low quantities of Ti, niobium, and Al elements. The mass amount of these alloying elements rarely constitutes more than 5% of the total mass amount. A similar is true for most Al alloys. Rather, SS structurally alone contains more than about 11% Cr. Most SS alloys contain Mn, Si, C, and Ni, as well as large concentrations of Ni or Mo [31]. The Fe-Cr phase diagram is shown in Figure 3.1

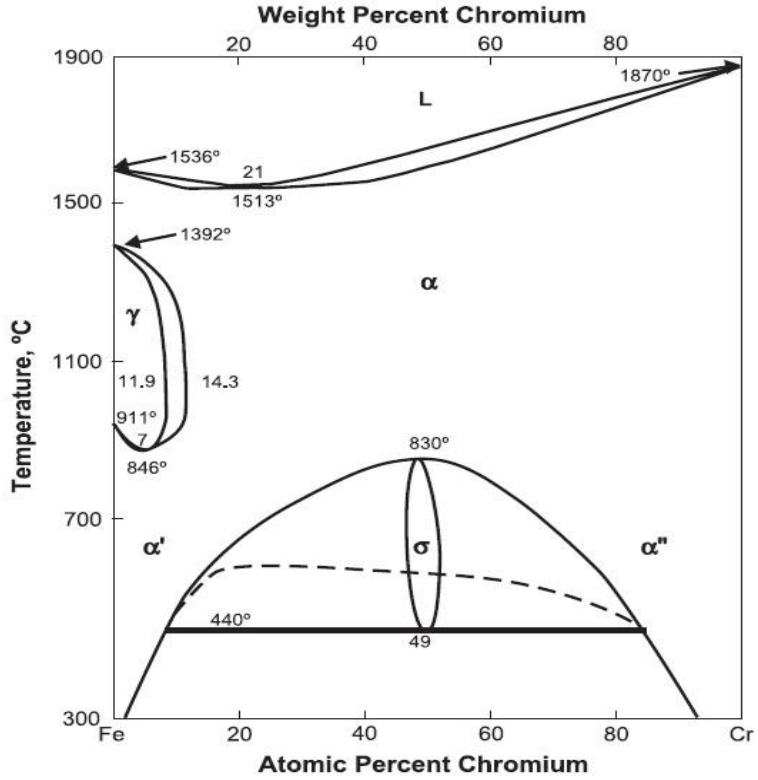

Figure 3.1. The Fe-Cr phase diagram [31].

3.1.1. Stainless Steel Phases

Although SS have 5 different product varieties, there are 3 main phase groups: ferrite, austenite and martensite, which form the microstructure and determine the general characterization of SS. In this section, these important phases are briefly mentioned.

Ferrite Phase (FP): It is the first line main phase group of SS. It has a BCC atomic lattice structure. The C solubility rate of ferritin at room temperature is 0.006%, and the C solubility rate at 723°C is 0.02%. The basic element of SS alloys is Fe. As noted, Fe solidifies as BCC cell-structured alloy before transforming into a denser FCC-cell structured austenite at lower temps. Even at lower temps, the BCC atom returns to the cell structure. It would not be wrong to conclude from this that both structures' free energy is close. It is the alloy elements that make a cell structure superior to the other, so the elements can change which one is dominant. Cr, which produces the passive film-forming ability that makes CoR of SS, has the ability to stabilize the BCC atomic cell structure. When the element Cr is added to the element Fe, at about 12% Cr, the

FP tends to shrink until it's stable at all temps. This is the proximate Cr grade required to prevent alloys from rusting below atmospheric conditions, but this impact isn't related to the atomic cell of the structure [31].

Austenite Phase (AP): The second major component phase of the SS alloy system is austenite. In the AP, the steel has a FCC atomic cell structure and the C solubility of the steel at 723°C is 0.8%. The maximum C solubility is 2.06%. The FCC structures are agreed to some transition metals to the right of Fe in the periodic table. Mentioned, the FCC must be considered normal for metals well below the melting temps as it is a more intensive structure. The existence of the BCC cell structure is known to be related to the electrons in the unpaired 3d orbital providing ferromagnetism. The addition of elements to the Fe element that reasons the pairing of electrons in 3d orbital reduces ferromagnetism and supports the FCC cell structure. Ni and Mn are the most significant alloy elements that do this, but C and N interstitial atoms are the strongest AP stabilizers for percent atoms. It is a fact that the uses of steels in the AP are limited by their solubility and tendency to form precipitating compounds with the Cr. Mn element has the ability to greatly promote N solubility. Hence, super AS such as S34565 use 4-6% Mn to allow 0.4 - 0.6% N levels to be achieved, resulting in higher pitting CoR [31].

In the hardening process of SS, the microstructure size of the AP obtained during the austenitization stage determines the material properties and material capacity to be obtained after heat treatment. The austenitization temps, the number of structural impurities, and the heating-waiting-cooling times are factors that affect the chemical composition of the produced material and thus the AP microstructure size.

Martensite Phase (MP): The MP is a phase consisting of a tetragonal or hexagonal atomic cell structure resulting from the diffusionless shifting of the AP. This atomic cell structure transformation can occur spontaneously during cooling or isothermally with externally applied forces and deformations. The MP is essentially a FP formed by the C supersaturation. The resulting microstructures are very thin and very imperfect. It consists of high tension interstitial atoms, as in C steel, and stresses occur in the cell structure due to interstitial elements. The resulting stresses impose the BCC

cell structure and try to put the cell into a tetragonal shape. This effect causes a dramatic increase in steel hardness in the MP [31].

In terms of MP formation, it is the most complex phase among the SS phases. Therefore, only a piece of brief information about this subject is given.

3.1.2. Comparison of Phases

For SS, while Cr is the alloying element that promotes the FP, none of the elements increase the quality of SS, although other elements have similar effects. Si, Al, Mo, W, Nb and Ti elements all support the effects of increasing the quality of the FP structure. C, N, Mn, Ni, and Cu elements don't extend the temps range in which the AP structure exists. Elements insoluble in Fe at AP temps, like impurities formed by elements such as P, K and O have no effect on which phase is preferred. It should therefore be underlined that the effect of an alloying element on the microstructure does not have any effect on its effect on CoR. Elements that support the FP structure against the AP structure also have encouraging effects, especially at very low temps, for intermetallic compounds generally composed of Fe, Cr, and some of these alloy elements.

The BCC cell structure of the FP allows austenite to diffuse faster than the FCC cell structure. This situation is valid for some elements' interstitial diffusion such as He, B, C, N, and O and rapid diffusion of all other elements. All elements' diffusion rate, both interstitial atomic structure and other structures, in the FP is about two or three times higher than that of AP. Thus, this means that precipitation reactions, although they may be in the AP, cannot generally be suppressed by quenching in the FP structure if they contain interstitial atomic elements. In the FP structure, intermetallic phases are formed faster. This becomes a problem just when the total Cr and Mo elements exceed about 20% of the phase diagram where the sigma phase appears. Therefore, this is a problem just for high Cr content alloys or for the FP structure of DS.

The FP structure has higher thermal conductivity and also lower thermal expansion than the AP structure. The strength value of the FP structure decreases with temps

more than that of the AP, but the high compatibility in thermal expansion between the FP and its oxide makes it an excellent high temps material. The FP structure has almost the same CoR as the AP structure, but the FP structure cannot take advantage of the benefits of this element because it cannot hold the N element in the solution. In DS, the FP is generally more CoR because it contains more Cr and Mo elements [31]. However, FS have lower properties than other SS in terms of strength, toughness, machinability, weldability and CoR. In addition, the critical prerequisite for orthopedically used implants is the complete absence of ferromagnetism. For these reasons, the microstructure of stainless steel implants must be fully austenitic, and thus FS and their alloys are in many respects unsatisfactory and unsuitable biomaterial candidates [34].

If we look at the differences between the MP structure and the other phases, the martensite structure in SS is limited to alloy levels where it can form at higher temps than the AP structure, but where austenite is unstable at normal temps levels. This limit gives the MP structure a rather narrow composition range. The lowest alloy grade in the MP is the alloy steel grade containing 0.1% to 0.2% C and 12% Cr. The highest alloyed MP structures are found in precipitation hardening phase structures. Therefore, the CoR of MS is inherently limited to a level no better than that of the 17-18% Cr alloy. If it is accepted that the Cr bonded as Cr carbide does not contribute to CoR, it would be very difficult for steel with MP structure at this level to be qualified as SS, but it is acceptable. The mechanical properties of MS contain the same types of properties as those of other alloy SS. The high content of alloy elements in MS provides an excessive hardening structure. The phase structure physical properties of martensite are very close to those of FP in the similar composition [31].

Historically, SS have been classified according to their microstructure and defined according to their austenitic, martensitic and ferritic phase structures. In addition, when the SS families are examined, there are two other SS families as duplex (austenitic plus ferritic) SS and precipitation hardenable stainless steels (PHS), which are based on the type of heat treatment used during production rather than microstructure [35]. Therefore, SS can be divided into 5 classes.

3.2. CLASSIFICATION OF STAINLESS STEELS

It was mentioned in the previous section that there are three main phase structures in SS, FP, AP and MP. SS microstructures can be obtained with different physical and mechanical properties by varying the alloy chemistry. Therefore, SS can be divided into 5 main classes from these three main phase structures. Compositions and links in SS alloys are shown in Figure 3.2.

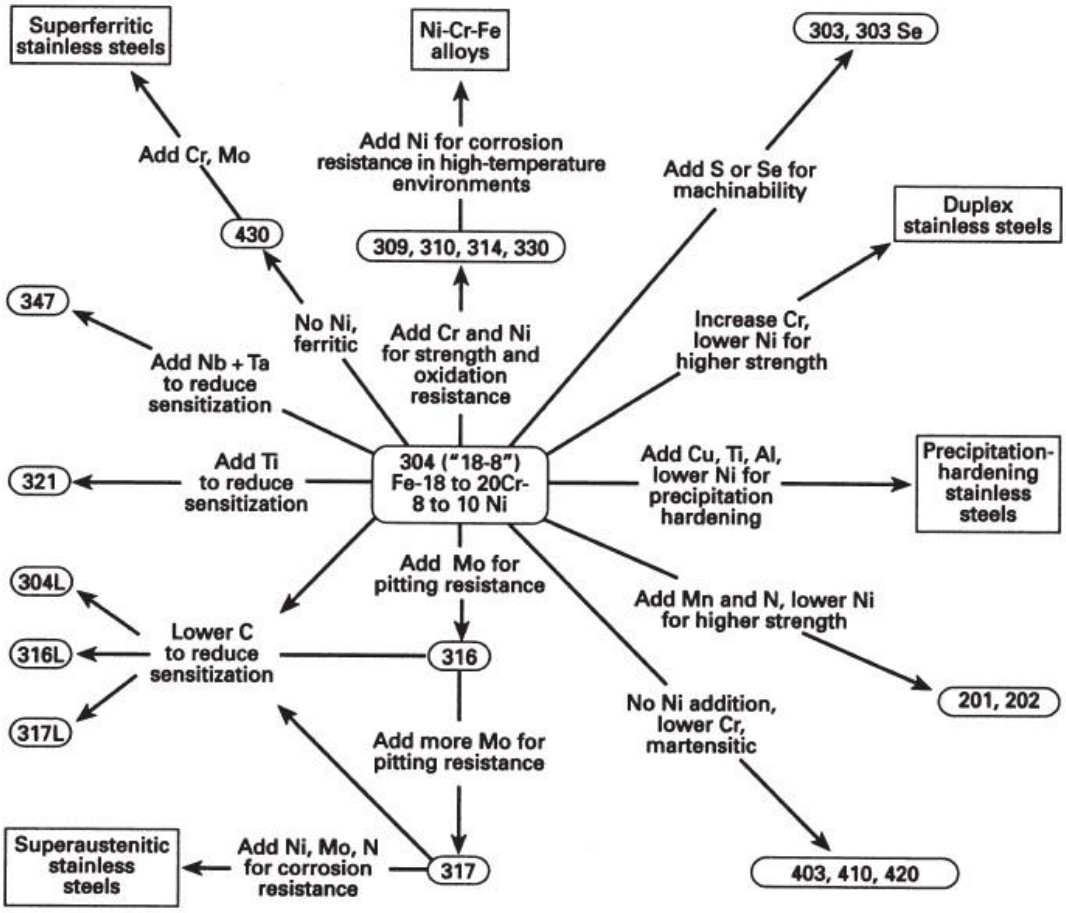

Figure 3.2. Compositions and links in stainless steel alloys [36].

5 main stainless steel classes are as follows;

a. Austenitic stainless steels (AS)
b. Ferritic stainless steels (FS)
c. Martensitic stainless steels (MS)
d. Duplex stainless steels (DS)

e. Precipitation hardening stainless steels (PHS)

SS grades have many different properties due to their different microstructures. For example, fully AP SS are not magnetic, but martensitic and ferritic phase SS have ferromagnetic structures. Many different properties of SS have been extensively studied in the industry for a very long time, and so much information is readily available in the literature [33].

3.2.1. Austenitic Stainless Steels

AS are the most common types of SS known, and also make up the largest family of SS in terms of alloy and use. They are recognized as the easiest non-magnetic SS to manufacture. They have very high formability and weldability and can be used successfully because they can withstand from cryogenic temps to the high temps of furnaces and jet engines. They contain among about 16% and 25% Cr and may also contain the element N in solution, which contributes to their high CoR in all of these ratios. It is thought that these alloys would have been even more widely used if the cost of Ni helping to stabilize AP structures had not been so high [31].

AS have many metallurgical advantages. AS can be made soft enough to be compatible with similar tools working with simple C steel, or they can be made incredibly strong by cold working up to yield strengths of over 2000 MPa. AS can have FCC structures that can be very hard or ductile down to absolute zero. In addition, they don't lose their strength as quickly as steel alloys with BCC cell structures in the FP at high temps. The least CoR varieties can resist the corrosive effects of the environments people encounter in their daily lives, while the most CoR varieties can even withstand boiling seawater [31]. Detailed information on AS is in section 3.3. It will be covered in detail.

3.2.2. Ferritic Stainless Steels

FS are the lowest cost SS alloys with high CoR and oxidation resistance. FS generally useful as light gauge plates as their toughness decreases rapidly under heavy loads. In addition, FS are one of the simplest types of SS. In their smaller forms, they contain

enough Cr to exceed natural C impurity levels and can reach the 11% Cr level required for steel rustproofing.

When the FS type 430 appeared in the early 20th century, the steels required a Cr level of 16% for achievable C removal to occur. Therefore, this process required a lot of Cr because during annealing, C combined with Cr to develop the fully ferritic structure, rendering the microstructure useless. The first commercial use of Ar-O decarburization in 1967 made a difference in FS production. This process, which only removed C without removing the element Ar and Cr of O, reduced the effects of C and N levels to levels that could be eliminated with minor Ti additions. This process is called stabilization and Ar-O decarburization has become indispensable in the structural production of FS. The C plus N level has been reduced from about 0.10% to about 0.04%, and cheaper high C ferrochrome is available instead of expensive low C versions. Therefore, there are two types of FS products available in today's industry. These are early high C types such as 430, 434, 436 and 446, and more modern balanced FS alloys led by 409 and 439 [31].

3.2.3. Martensitic Stainless Steels

The smallest category in the use of SS in the industry is MS and its alloys. The main reason for this is that the CoR of MS alloys is very limited due to the need to keep the alloy grades low to produce the MP structure. However, today they fill an important gap as stable, high-temperature SS alloys with a strong, hard, and tough microstructure with very good CoR. The usable alloys of martensitic stainless steel superficially contain 11-18% Cr and 1% C. Relatively smaller amounts of Ni, Mo, W, V and Nb may also be added from time to time. There are also MS in which elements such as Cu and Ti are added to the alloy structure to provide greater hardness by precipitation [33].

MS are a family of SS with exceptional CoR among all stainless alloys. The requirement to be completely CoR AP structure tends to limit the amount of Cr and Mo they can contain. Most of the C element in them forms Cr carbides, removing the effective Cr content. These resulting limitations make it possible to make the good

properties of MS usable only in smooth environments compared to other SS. Partly because of their low cost, high strength, and hardness, they make them a very useful stainless steel material [31].

Simple structured MS don't have a different aspect that is not directly applied to MS with stainless ability. The expected negativities related to MS with stainless ability are mainly due to the strong ferritizing effect of the element Cr. The element Cr in alloys has a supporting effect on the formation of FP structure, which limits the temps and composition ranges at which it is possible to obtain a fully AP structure to form a MP structure [33]. The being of FP structure in a MP structure has a negative effect on the mechanical properties of steels such as strength, hardness, and toughness. The FP structure may appear in the steel casting structure and may occur during austenitizing or tempering. All the usual negative effects inherent in MS alloys such as tempering embrittlement, residual austenite etc. are still present today.

3.2.4. Duplex Stainless Steels

The newest family of SS materials is DS and DS alloys. Its microstructure consists of mixtures of FP and AP structures. The combination of FP and AP in their structures gives alloys higher strength than either phase alone. DS alloys contain at least 20% Cr, so these products are considered alloys with high resistance to corrosion and its effects. However, they cannot be used at very high temps values due to embrittlement phases. Their low Ni content makes them more economical than AS with the same level of CoR. It is foreseen that this family of SS will largely replace stainless alloys such as AISI 316L and AISI 317L in the further [31].

3.2.5. Precipitation-Hardening Stainless Steels

PHS are a family of very high-strength SS with good CoR. In no case is the CoR found in PHS better than AISI 304 SS. Where high strength and very high CoR are required in the manufacture of a product, the designer or engineers should be familiar with PHS for optimum material properties. It takes advantage of the low AP stability in Cr/Ni SS by making PHS and alloys so lean that they can be converted almost fully to MP

by a thermal or mechanical process. This MP structure can then be over hardened by co-precipitation of intermetallic alloys, elemental Cu, nitrides, and phosphite. This PHS can also be done to form a fully AP cell structure, which also provides a PHS alloy. However, martensitic precipitation-hardened phase structures are much more widely used. The boundary between high-alloyed MS, which undergo a secondary hardening during tempering, and PHS alloys is an unclear situation [31].

3.3. AUSTENITIC STAINLESS STEELS AND ALLOY FAMILIES

AS are the most common types of SS known, and also make up the largest family of SS in terms of alloy and use. They are recognized as the easiest non-magnetic SS to manufacture. They have very high formability and weldability and can be used successfully because they can withstand from cryogenic temps to the high temps of furnaces and jet engines. They contain among about 16% and 25% Cr and may also contain the element N in solution, which contributes to their high CoR in all of these ratios. It is thought that these alloys would have been even more widely used if the cost of Ni helping to stabilize AP structures had not been so high [36].

AS have many metallurgical advantages. AS can be made soft sufficient to be compatible with similar tools working with simple C steel, or they can be made strong by cold working up to yield strengths of over 2000 MPa. AS can have FCC structures which can be very hard or ductile down to absolute zero. In addition, they don't lose their strength as quickly as steel alloys with BCC cell structures in the FP at high temps. The least CoR varieties can withstand the corrosive effects of the environments people encounter in their daily lives, while the most CoR varieties can even withstand boiling seawater. Therefore, AS grades are the most widely used SS grades because in most cases they provide predictable and high levels of CoR combined with good mechanical properties. AS alloys can be basically divided into three groups [36].

a. A group of lean alloys such as 201 and 301 SS. They are usually the preferred SS when high strength and high formability are the primary goals. Because the lower but adjustable AP stability of these alloys provides a wide range of material hardness and high ductility. Richer alloys like 305 with minimal strain

hardening have a high alloy, low strain hardening ratio for this aim. Among the alloys used for general use, 304 SS is in this group.

b. Steel alloys with Cr-Ni content to prevent oxidation at high temps. This group can be brought to a higher level with Si and rare earth elements. If the process requires high-temps resistance, C, N, Nb and Mo can be added to the structure of the alloy. 302B, 309, 310, 347 and SS alloys with various properties are in this group.

c. SS alloys containing Cr, Mo, Ni and nitrogen where CoR is the main target. If desired, elements such as Si and Cu can be added to the alloy content for durability. This group includes 316L, 317L, 904L and SS alloys with various properties.

AS alloy families are shown in Figure 3.3.

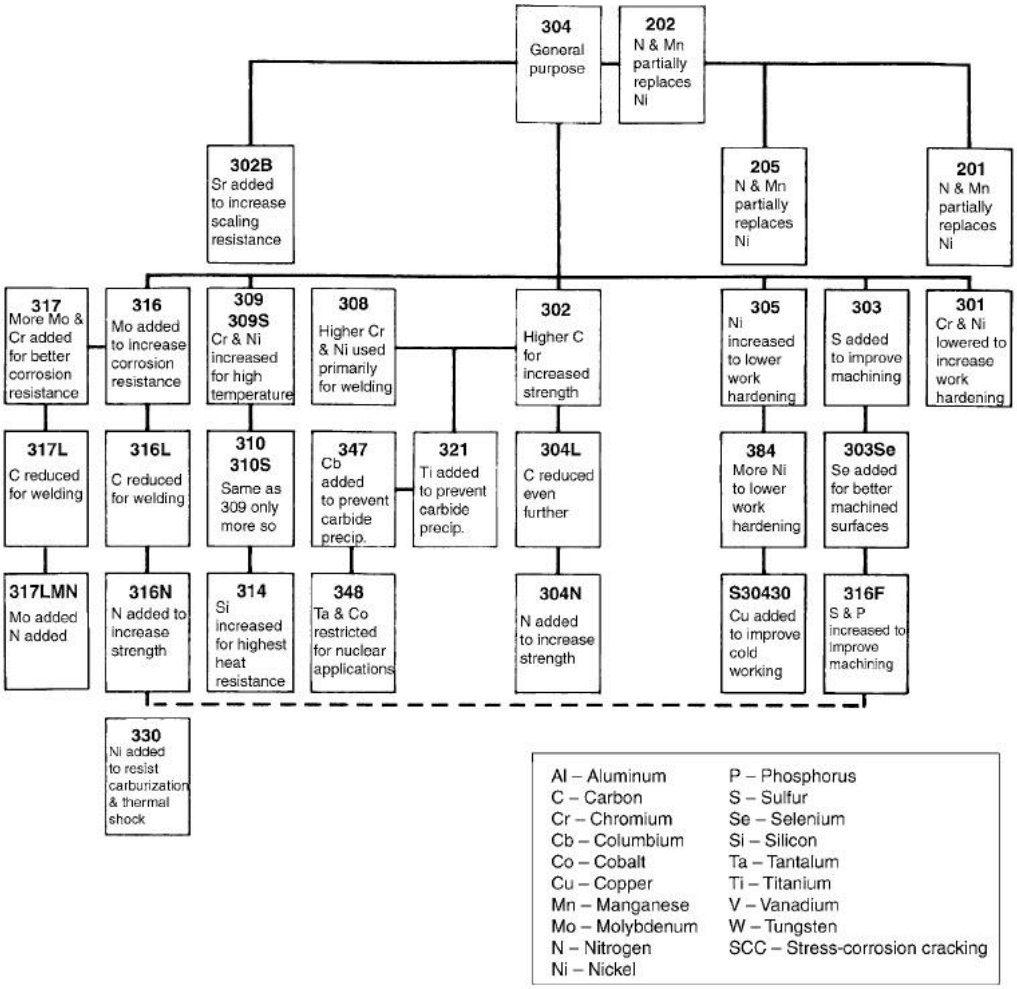

Figure 3.3. Austenitic stainless steel alloy families [31].

In the next section, austenitic stainless steel alloys, where CoR is the main objective, are examined.

3.3.1. Corrosion Resistant Austenitic Alloys

SS are often the materials of choice for their CoR. Under normal atmospheric conditions, SS containing more than 10% Cr become rustproof. AS require higher amounts of Cr than this to stabilize the AP structure at room temps. Therefore, there is a thought that they are superior in CoR. The biggest advantage of alloys in the AP structure is their ability to use N, which is a cheap and powerful alloying element. Such are the key properties of the more modern AS that have come into use in the last two decades.

The chloride ion is abundant all over the world and is the most aggressive ion against SS. The chloride ion, which is especially abundant in seawater, is also found in rain, food, roads, and even human bodies. Chlorides tend to degrade the oxide film in SS. Active corrosion begins to occur on SS surfaces if the chloride's activity level, temps and acidity conditions are effective enough to break up the oxide film. If the areal weakness in the oxide film is quite intense, pitting begins on the material. Such pitting may be passive and unstable, or it may increase incessantly. Chemically, other halides may have a similar impact, yet this is less common [33].

Due to the almost ubiquitous presence of the chloride ion, CoR of AS can be considered to be designed to withstand chloride pit attack. The pitting condition that occurs in SS is in many cases the first threshold of corrosion. However, crevice corrosion is more destructive and often limits the designs that can be produced against corrosion. Formed cracks can be found not just in joints but also under paint films, welding spatter, environmental deposits. There is also environments where resistance in steels occurs in different conditions such as bases, organic and oxidizing acids, but these environments are not the acceptable exceptions. The higher the Cr element content and amount of an alloy, the easier the Cr reservoir ready to form the Cr film layer. The roles of Mo and N in the alloy are more uncertain and controversial than the element Cr. It was explained that the basic element Cr in the structure of AS is highly reactive and can form compounds with C, O, S and other transition elements. Unless the regions where Cr is positioned to form the phase structure rich in Cr content, the alloys will remain poor in Cr unless subjected to homogenization annealing for long periods [31].

The passive layer formed by the Cr element is very thin in proportion to the oxide layers, with a thickness of about 1 - 10 nm. Passive layer formation does not cause depletion of the amount of Cr under the film, as occurs in oxide layers. As the content of Cr and Mo in alloy increases, the film becomes thinner, and therefore the density necessary to form the passive film decreases. Corrosion and other impact-resistant AS grades range from AISI 316L to high Mo and high N alloys that have been commercialized in recent years. The most notable of this stainless steel group are listed in Table 3.1.

Table 3.1. Compositions of the most commonly used austenitic alloys [31].

Alloy	Designation	C	N	Cr	Ni	Mo	Mn	Si
201	S20100	0.08	0.07	16.3	4.5	0.2	7.1	0.45
201 drawing	S220100	0.08	0.07	16.9	5.4	0.02	7.1	0.5
201LN	S20153	0.02	0.13	16.3	4.5	0.2	7.1	0.45
301 tensile	S30100	0.08	0.4	16.6	6.8	0.2	1.0	0.45
301 drawing	S30100	0.08	0.04	17.4	7.4	0.02	1.7	0.45
303	S30300	...	...	...	...	...	...	...
304	S30400	0.05	0.05	18.3	8.1	0.3	1.8	0.45
304 drawing	S30400	0.05	0.04	18.4	8.6	0.3	1.8	0.45
304 extra drawing	S30400	0.06	0.04	18.3	9.1	0.3	1.8	0.45
304L tubing	S30403	0.02	0.09	18.3	8.1	0.3	1.8	0.45
305	S30500	0.05	0.02	18.8	12.1	0.2	0.8	0.60
321	S32100	0.05	0.01	17.7	9.1	0.03	1.0	0.45
316L	S31603	0.02	0.0	16.4	10.5	2.1	1.8	0.50

Developments in the SS industry are rapid and today SS has become a suitable material for many applications where Ni-based or Ti alloys were previously used. It is not difficult to envision alloys that contain less Ni and Mo than AISI 316L, are completely resistant to intermetallic phase precipitation, and are much more resistant to stress corrosion cracking due to higher AP stability.

In the next section, the use of high CoR SS as biomaterials is investigated.

3.3.2. Use of Corrosion Resistant Stainless Steels as Biomaterials

SS materials are often used as biological materials to replace or repair the structural components of the human body. The reason for this is that they have superior fatigue strength, tensile strength, and fracture toughness when compared with polymeric and ceramic materials. Therefore, SS biomaterials are used in medical products such as bone plates, artificial joints, intramedullary nails, screws, spinal fixations, spinal spacers, pacemaker sheaths, external fixators, wires, artificial heart valves, stents, and dental implants. CoCr alloys, commercially pure Ti, Ti6Al4V alloys, and AISI 316L SS are typical metallic biomaterials used as implants. Although initially used for industrial aims, these materials have been tested as biomaterials due to their excellent mechanical properties and high CoR.

It is important to distinguish between SS grades such as AISI 303, AISI 304, and AISI 316L used for medical applications and commercial grade SS used for other medical devices. Europe defines medical devices as devices exposed to human tissue for more than 30 days. Thus, by this definition, it means that SS used as biomaterials will be in contact with human tissue for more than 30 days. For instance, 316L SS pins are used with fixation devices to repair damaged bones. These pins pass through the skin or the underlying tissue and are fixed to the bone from both sides of the damaged part and the application is performed [37].

The ISO 5832-1 and ISO 5832-9 standards specify forged SS and high N content SS, respectively, for implants used for surgical purposes. These materials were originally developed from AISI 316L. In addition, implant-grade SS such as AISI 316L must have special properties for resistance to pitting corrosion and cleanability not applicable to other SS. Therefore, special production routes are used for the production of "clean" implant SS. The ISO 7153-1 standard deal with SS specifications for dental and surgical instruments. It should be emphasized that the definitions in the ISO 7153-1 standard are general information. This standard also specifies typical application areas for all SS families. At the same time, all of these standards are used by all dental and surgical equipment manufacturers around the world to set product standards [37].

AISI 303 is used in medical devices, where its free-machining ability has an increasing effect on the ease of production. Examples of this are medical products such as drilled or punched screws. Parts of multi-part dental instruments are often manufactured with the material AISI 303 SS. It should be noted that low CoR is not a disadvantage in this application. AISI 304 SS are applied in medical instruments where good CoR and relatively lower strength are required. Most of the instruments used in these applications come into temporary contact with patients [37].

SS generally used in medicine are AS with chemical properties containing 17-20% Cr, 12-15% Ni, 2-3% Mo and fewer amounts of other elements. Cr is the main element liable for the high passivation in SS [36]. One of the preferred requirements for orthopedically used medical materials is the complete absence of ferromagnetism. Since the only SS family that meets these conditions is AS, they are widely used as

implants. In particular, AISI 316L has acceptable biological compatibility and properties suitable for high load-bearing conditions. This has made AISI 316L a preferred surgical implant material [38].

It has been mentioned in the previous sections that there are three main types of microstructures in SS; FS, AS and MS and that these microstructures can be obtained by properly tuning the steel chemistry. In the next section, information about AISI 316L, which is the focus of this study, will be given.

3.4. AISI 316L STAINLESS STEEL

While making definitions about AISI 316L SS, it is absolutely necessary to mention AISI 316 stainless steel. AISI 316 and AISI 316L are austenitic SS with a Cr-Ni Mo content developed to provide CoR in moderately corrosive environments. They are mostly used for processes in environments containing chlorides or halides. The low C chemistry of AISI 316L, which is chemically combined with the addition of N, allows it to easily meet the mechanical properties of the main SS, AISI 316 steel. AISI 316L alloy has a high ability to resist atmospheric corrosion as well as oxidizing and reducing environments. In addition, this alloy exhibits excellent resistance to intergranular corrosion in the welded condition. AISI 316L alloy has good strength values and toughness at cryogenic temps, while it is non-magnetic in the annealed condition. In addition, AISI 316 and AISI 316L are easily weldable as well as being machined with standard workshop fabrication practices [39].

Annealing, a process to reduce hardness, increases the ductility of the material as well as its plastic deformation ability. AISI 316 and 316L SS alloys require heat treatment between 1,038 and 1,149 degrees Celsius before quenching rapidly. On the other hand, 316L is a better choice for a project that requires a lot of resources. This is because AISI 316 is more susceptible to weld corrosion than 316L. The physical properties of AISI 316L are shown in Table 3.2.

Table 3.2. The physical properties of AISI 316L [36].

Physical Property	
Density (kg/m³)	7,9 x 10 ³
Modulus of Elasticity (GPa)	193
Poisson Ratio	0,25
Specific Heat (J/kg K)	500
Thermal Conductivit (W/mK)	
100°C	16,2
500°C	21,5
Melting Range (°C)	1375 – 1400

3.4.1. Phase Transformation in AISI 316 Stainless Steels

AS are widely preferred in many industrial applications and therefore have an important place in controlling microstructure development, mechanical and physical properties. Plastic deformation of such materials can cause the AP structure to transform into a martensite structure. In AS, the deformation process can induce the formation of two types of MP structures [40].

Austenite γ (FCC)→ martensite ε (HCP)→ martensite α'(BCC)

On the other hand, the direct transformation γ α' through dislocation reactions was found to be possible. However, it is also suspected that ε -MP at fewer temps (<-50ºC). Processing parameters, for instance, stress state, temperature which is associated with rate of deformation can have a strong influence on the amount of ε as well as α' martensite. Also, great influence is the steel composition also stacking fault energy [40].

Eichelman which is associated with Hull have developed an equation which gives as, α'MP formation temps Ms;

$$Ms(\%C) = 1302 - 42(\%Cr) - 61(\%Ni) - 33(\%Mn) - 28(\%Si) - 1667\,(\%[C + N]) \quad (3.1)$$

The necessary energy for the MP transformation is supplied via the plastic deformation process. The supplied energy can increase the temperature of martensite formation to Md which is the temps below which MP will form under deformation. Angel et al, have studied the temps with composition for diverse SS as well as formulated Equation 3.2

$$Md(30/50)(\%C) = 413 - 13.7(\%Cr) - 9.5(\%Ni) - 8.1(\%Mn) - 18.5(\%Mo) - 9.2(\%Si) - 462(\%[C+N]) \quad (3.2)$$

Md is the temps limiting martensitic transformation due to deformation, which is not associated with any MP that may form above this temperature. Martensitic transformation is expected to change through stress states. [40].

3.4.2. Welding Capacity of AISI 316L Stainless Steel

It has been mentioned that AISI 316L SS is ideal for operable medical device applications due to its high CoR and non-magnetic properties. A number of different joining methods can be used to fabricate components of AS, each offering different advantages. RSW is a popular welding process because it is associated with low cost combined with its repeatability at high speeds and is also a convenient method for joining small-scale components [41].

O in the air can have the effect of bonding with molten metal to form a thick oxide layer on the properties of the welded steel. Moreover, there is a possibility that C interacts with Cr, causing carburization. In addition, this process reduces the CoR of the welded metal. Therefore, while hydrogen causes a porous structure in the weld area, copper and lead can cause brittleness in the base metal. It is possible to control the austenite stabilization, which is important for preserving the structure and general properties of the SS after welding, through the basic components of the alloying elements used in the alloy. Negative effects during welding can be eliminated by providing austenite stability. Cr, Ni, Mo, C, nitrogen and Mn can be given as examples of elements that help austenite to be stable after welding [41].

PART 4

RESISTANCE SPOT WELDING

RSW was invented by Elihu Thomson in 1877 and has been widely used since then as a manufacturing process for joining sheet metals. Although RSW is more than 100 years old, the physics of the process is not fully understood; however, this has not prevented its industrial application for joining various metals with each other [42]. RSW is a popular welding process today because of its high speed associated with the low cost combination. It also provides excellent repeatability. RSW is one of the key metal joining techniques for high volume production in the automotive, biomedical and electronics industries [43].

RSW is a method of joining sheet metals together by melting, using high heat generated by the resistance, which is created by applying pressure to two or more metal sheets on top of each other, between two copper electrodes with high conductivity, and passing low voltage high current with certain repetitions. This welding method is simply applied in three steps: compression, welding and holding. Firstly, in the compression step, the welding device applies the desired amount of pressure to the sheets to be applied through the electrodes connected to the pneumatic arms. In the second step, the welding step, the welding device applies current to the pressurized points of the sheets through electrodes with high conductivity. With the application of the current, the current passes through the sheets for a certain period of time and heat is released on the sheet surfaces where the resistance is high. With the heat released, a molten metal pool (nugget) is formed between the sheets. The interruption of the current means the start of the last step, the holding step. In this step, the molten metals on the sheet surfaces become solid by cooling with the effect of the cooling liquid and air passing through the electrodes. Thus, the welding process is

completed [44]. RSW construction stages are shown in detail in Figure 4.1

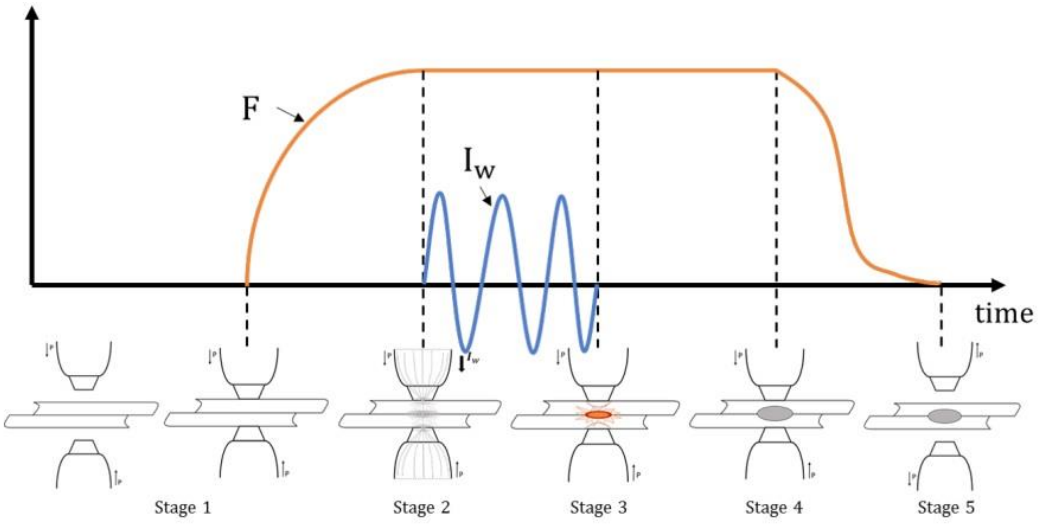

Figure 4.1. Resistance spot welding cycle showing the main phases of the process [45].

The electrical RSW process, used to join multiple materials at their common interface, is a complex interaction of thermal, mechanical, electrical, metallurgical and surface phenomena. If a specific example is given for this situation, the water-cooled copper electrodes used during the welding process can be given as an example. Water-cooled copper electrodes basically provide three functions [42];

a. Low electrical resistances provide a channel to carry the high current to the workpiece to be treated without significant thermal losses.
b. Thanks to its high thermal conductivity, it transmits heat to the workpiece to be applied and allows to control the formation of nuggets and cooling.
c. Electrodes exert an intense force on the outer surfaces of the materials to be welded.

The two most important elements in the RSW method are resistance and resistivity. Resistivity is a physical property that expresses the resistance of the material to be applied to the electric current and is independent of geometry. Resistivity is a physical expression expressed by the resistivity and geometry of the material.

The resistance equation is as in equation 4.1.

$$R = \rho l / A \tag{4.1}$$

In this equation, ρ is the resistivity, l is the length of the conductor, R is the resistance and A is the cross-sectional area of the conductor.

The resistivity of the electrodes and materials is very important in order to generate heat on the right spot in RSW. A decrease in resistivity means that the resistance will also decrease, thus increasing the conductivity. It is difficult to join materials with high conductivity, such as Al, with the RSW method, since the current will pass without difficulty at the points where the conductivity is high. Another important factor is the surface contact resistance. The surface contact resistance depends on the surface conditions of the sheets to be welded and the force applied by the electrode. Figure 4.2 shows the contact points in the RSW method.

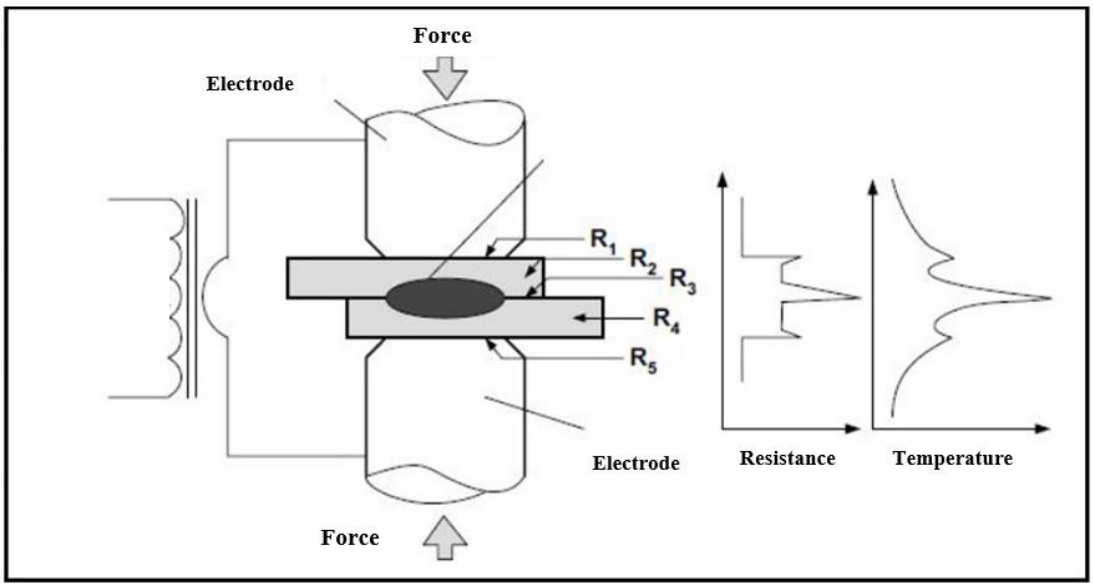

Figure 4.2. Contact points in the resistance spot welding method [46].

It is desired that the conductivity of the electrodes is higher so that the highest contact resistance is formed in the R3 region and the heat generation due to the resistance in the R1 and R5 regions is low. The R3 resistance region is the major region as determines source nugget formation [46].

The resistance changes rapidly during the welding process, so the resistance is considered to have dynamic effects. For quality welding, a resistance change graph can be created by monitoring the resistance change during the RSW process. An example graph is shown in Figure 4.3

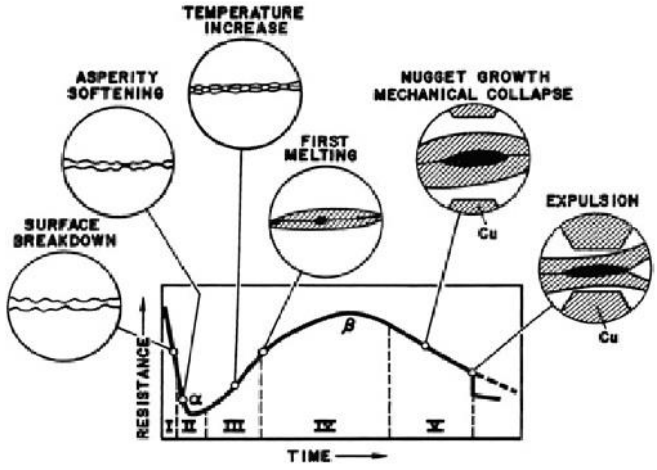

Figure 4.3. Typical dynamic resistance curve for spot resistance welding of steel [46].

As can be seen in the graph, initially, the resistance is high because surface oxides and rough surfaces create high resistance to the flowing current. With sufficient pressure and heat, the resistance decreases as a result of the fragmentation of the oxides and the reduction of the surface roughness. As the process continues, the heat generated and the surrounding area of the metal heat up further, increasing the resistance significantly and the mass resistance of the plates becomes dominant. Then, the heating process by mass resistance increases enough to form a molten pool. With the expansion of the molten pool, the path taken by the electric current expands and the current density decreases, the resistance reaches its maximum value and decreases again. In addition, there is a possibility that the formed indentations can significantly reduce the resistance [11].

4.1. WELDING CURRENT AND TIME

The heat generated during the RSW process is directly proportional to the square of the current and time. Although the two parameters are responsible for heat generation, the rate of heat generation is dependent on the welding current. This is because the

amount of heat lost increases with increasing time. The equation giving the amount of heat produced is as in equation 4.2.

$$H = I^2.R.t \tag{4.2}$$

Here, H is the heat produced, I is the applied welding current, t is the welding time (period), R is the resistance.

Increased heat loss during the welding process increases heat-affected zone formation and the amount of thermal degradation. The level of current required for any metal material is inversely proportional to its electrical and thermal resistance. The weld size also increases with increasing welding current during the welding process. However, with increasing welding current, the welding time should be reduced to prevent negative effects such as excessive electrode indentation, spatter, and electrode tip distortion [11]. While the welding current can be from 20kA to 100kA for light alloys, it is used at values between 4 and 20kA for steels. Welding time depends on the type of material and surface coating. Welding current cycles may differ depending on the product material. [44].

4.2. ELECTRODE FORCE

As the increase in the electrode force increases the contact on the sheet surface, it significantly reduces the resistance, causing the surface oxides and the coating to move away from the area. Almost all metals have roughnesses on their surfaces that limit the contact area of sheet materials. As soon as the current is applied to the sheets, the electrons are forced to pass through these roughnesses that come into contact with each other. Thus, local increases in current density occur due to increased resistance. As the electrode strength increases, these roughnesses, which increase the resistance, are removed. This means that the heat produced will be less. The removal of surface impurities and oxides with the increase of the electrode strength shows the same effect in reducing the contact resistance [11].

In addition to these, some of the electrode force is spent to balance the molten metal liquid pressure [44]. In cases where the pressure cannot be balanced, splashes occur. There are basically two mechanisms that bring about the jumping event. The first mechanism occurs when the welding current and welding time are high as well as the pressure applied by the electrode. The second mechanism is due to insufficient electrode strength. During the RSW process, if the pressure of the weld metal is higher than the electrode force, spatter occurs as the expansion continues.

4.3. METALLURGICAL AND PHYSICAL EFFECTS OF RESISTANCE SPOT WELDING

Welding is a metallurgical process. Since the welding process at high temperatures causes microstructural changes in and around the welding area, it disrupts the grain homogeneity of the application materials. Therefore, mechanical performances different from the mechanical properties of the metal are observed in and around the weld area. The nugget areas after the welding process are shown in Figure 4.4.

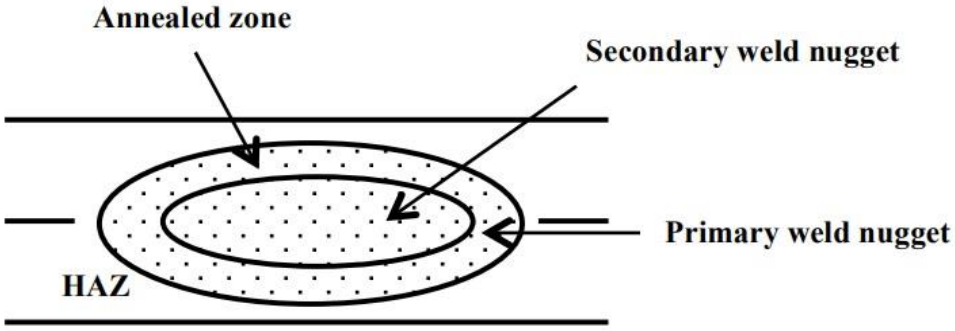

Figure 4.4. The nugget areas after the welding process [47].

There are three distinct macrostructural regions in the junction region at the end of the RSW. The first of these macro-structural regions is the weld area, which melts and solidifies during the RSW process and therefore exhibits a cast structure. It is governed by heat input depending on RSW parameters such as welding time, welding current and electrode force, respectively. Weld size, defined as the directional width of the weld zone between sheets, is one of the most important factors in determining the quality of spot resistance welding. The second of the macro-structural regions is the

region under the influence of heat, where melting is not observed, but is exposed to micro-structural changes due to the heat generated. The heat affected zone significantly affects the welding performance. The size of this zone depends on the heat loss from the source zone to the environment. The third region, which is the last of the macrostructural sections, is the base metal region where no microstructural changes are observed. [47]

Sudden heating and cooling caused by thermal cycles during RSW can cause significant changes in the microstructure, resulting in large differences in the hardness profile. The two most important factors affecting the microstructure development and hardness characteristics of RSW are chemical composition and cooling rate [44].

The factors affecting the chemical composition are the composition of the weld area and the chemical composition of the base metal involved in the composition. The melting rate of each sheet is different in different thicknesses or welding of different metal parts. Of the parts to be welded, the one with higher electrical resistance or thickness contributes more to the weld zone volume [48].

The strength mismatch between the metal to be welded, the heat-affected zone, and the base metal cause a strain concentration to occur in the region with the lowest strength. In addition, joint notch and indentations caused by electrode force may occur after welding, which causes stress concentrations that reduce the load-bearing capacity of the welded areas compared to the base metal [49].

Another defect that may occur after welding is the gaps formed during welding. The formation of weld voids can occur with two effects. One of these effects is spatter and the other is the shrinkage of the weld metal during cooling. The material ejected from the weld zone due to the first effect, spatter, causes the formation of cavities in the weld zone by solidification of the molten metal. In the second effect, the shrinkage of the molten metal in the weld area causes the formation of gaps as a result of the separation of the surfaces between the parts. If the electrode force during cooling is high enough, the formation of voids or pores in the weld can be prevented. The reason for this gap formation is that the electrodes are released before the weld pool

completely solidifies. In welding processes, voids are usually formed in the center of the weld zone, where solidification occurs last [48].

4.4. MECHANICAL PERFORMANCE OF RESISTANCE SPOT WELDING

The mechanical performance of RSW is generally evaluated under static/semi-static, fatigue and impact conditions. Although most RSW are damaged under fatigue conditions, excessive load on welds due to poor quality welding processes can cause damage to the welded areas [48].

RSW joints are subjected to both shear loading and welded sheet tensile loading due to relative displacement or rotational motion of adjacent sheets. In the light of these effects, mechanical tests are carried out under different loading conditions in order to determine the mechanical behavior of RSW parts. The most commonly used tests are the cross-tensile and tensile-shear tests. The tensile-shear test on the point welded joint aims to determine the tensile loading in the welded region, and the cross-tensile test aims to determine the tensile loading conditions created by the tensile loading [48].

4.5. FRACTURE TYPES IN RESISTANCE SPOT WELDING REGIONS

It can be assumed that it refers to the mechanical property of the fracture type that occurs in the parts welded in a resistance spot welding process. In point resistance welded joints, 4 different fracture types are generally seen. These are respectively; interfacial damage type fracture, tensile type fracture, partial fracture and partial thickness-tensile fracture. Its features are briefly given below [48].

a. In the interface damage type, the fracture occurs along the weld zone. It is an undesirable type of fracture in the automotive industry, as it is thought to have bad effects on collision resistance.
b. The damage that occurs in tensile type fracture occurs from the welding zone towards the sheet metal. The crack formed in this type of damage may occur between the base metal and the heat affected area or between the weld metal and

the heat affected area depending on the loading conditions as well as the geometric and metallurgical properties of the weld area.

c. In the case of partial fracture, the crack that occurs starts in the weld area and progresses through the sheet thickness.
d. In partial thickness-tensile fracture, the inclined crack advancing to the weld zone causes breakage from a part of the sheet thickness.

Fracture types significantly affect the load carrying capacity and energy absorption ability of RSW parts. Due to its high absorption and plastic deformation properties, it is preferred to see tensile type damage on weld surfaces with RSW compared to others. The quality control of tensile fracture is mentioned in the literature, where the same weld can transmit higher forces, thus causing more severe plastic deformation in adjacent parts during fracture, thereby distributing the strain concentration [46]. Therefore, welding processes should be performed at welding parameters where tensile fracture will occur. Therefore, it is very important to examine the RSW applicability capabilities, especially in SS alloys. In addition, this issue is very important for SS where complex microstructural transformations such as softening in the heat-affected zone and formation of hard and brittle phases in the weld zone are observed as a result of welding processes. Therefore, the effects of RSW applied on AISI 316L samples were investigated in this study.

PART 5

TENSILE TEST

Tensile Test is an engineering and materials science test, in which a force is applied to a sample under a load with controlled tension up to a certain level or until the material breaks completely and to determine the behavior of the sample. Tensile testing is one of the most common mechanical testing techniques, measuring how strong a material is and how much it can be stretched before breaking. This test method is used to determine yield strength, ultimate tensile strength, strain hardening characteristics, Young's modulus, Poisson's ratio, and degree of ductility [50].

For industrial reasons and the testing are easy, several material properties are based on measurements made in the tensile test. Specific, or nonbasic tensile test properties are mostly used, they will be characterized at this stage and some description is given of their impact on processes, even though this can only be done qualitatively. Figure 5.1 shows a tensile test piece

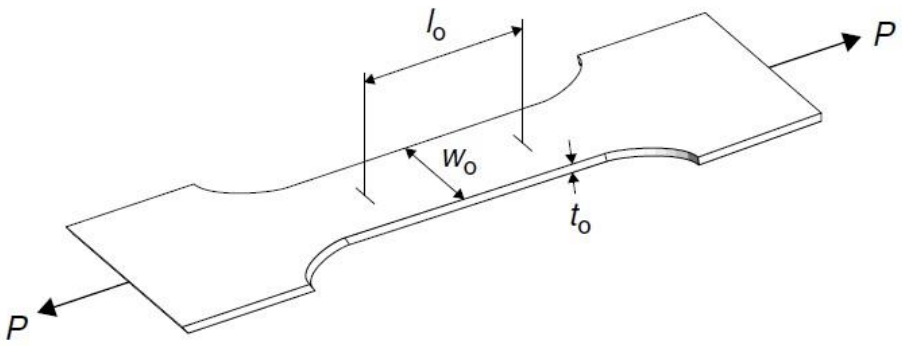

Figure 5.1. Tensile test strip [50].

This is a typical standard test samples example of a parallel, reduced cross-section for a length of at least four times the width, ω_0. The initial thickness is t_0 and the load on the piece,P, at any instant, is measured with a load cell in the tensile machine. In the

mid of the sample, a gauge length l_0 is followed by an extensometer, and the gauge length l available at any one time is $\Delta l = l - l_0$. In some tests, a transverse extensometer can also be used to measure the change in width, i.e. $\Delta\omega = \omega - \omega_0$. During the tensile test, the payload and extension will be recorded in a data collection system and a file will be created; this is then analyzed and various material property diagrams can be generated. Some of these are described below [50].

5.1. THE LOAD–EXTENSION DIAGRAM

Figure 5.2 shows a representative load-extension diagram for a test on a tensile drawing steel sample

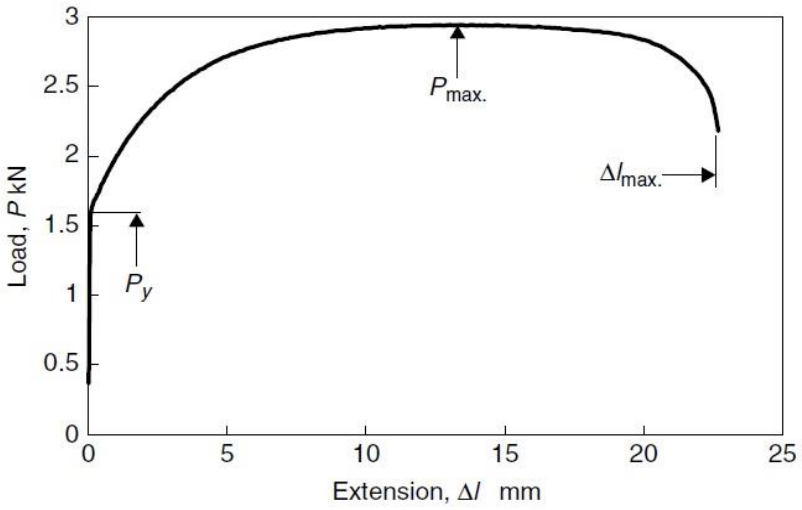

Figure 5.2. Load–extension diagram for a tensile test of sheet steel [50].

The elastic extension is very tiny that it cannot be seen. P_y is the initial yield load, at which plastic deformation begins. The initial yield is followed by an area in which the deformation or extension in the lane is uniform and the increasing load. The increasing load is because of strain hardening, exhibited by most metals and metal alloys in the soft state, where the strength or hardness of the material increases with plastic deformation. During strain-hardening, the cross-sectional area of the strip grows down while the length grows up. The strain-hardening impact is only offset by the rate of growth down in the area and the load achieves a maximum P_{max}. After this, deformation in the lane stops to be uniform and a spread neck improves in the

decreased area; non-uniform extension continues within the neck until the lane breaks [50]. The extension at this instant is l_{max} and a tensile test characteristic known as the total elongation can be calculated. This is defined by this equation

$$E_{tot} = \frac{l_{max} - l_0}{l_0} \; x \; 100\% \tag{5.1}$$

5.2. THE ENGINEERING STRESS–STRAIN DIAGRAM

Before the improvement of information processing systems it was usual to measure the load–extension diagram by dividing the load by the initial cross-sectional area, $A_0 = \omega_0 . t_0$, and the extension by l_0, to get the engineering stress-strain curve. Thus had the benefit that a diagram was got which was independent of the initial dimensions of the test piece, but it was still not a true material property curve. Throughout the tensile test, the cross-sectional area will decrease so that the true stress on the material will be nicer than the engineering stress. The engineering stress-strain diagrams are still well used and several properties are reproduced from them. Figure 5.3 illustrates the engineering stress-strain curve calculated from the load [50].

Engineering stress equation is,

$$\sigma_{eng} = \frac{P}{A_0} \tag{5.2}$$

Engineering strain equation is,

$$e_{eng} = \frac{\Delta l}{l_0} \; x \; 100\% \tag{5.3}$$

Initial yield stress equation is,

$$(\sigma_f)_0 = \frac{P_y}{A_0} \tag{5.4}$$

The maximum engineering stress (ultimate tensile stress / tensile strength);

$$TS = \frac{P_{max}}{A_0} \tag{5.5}$$

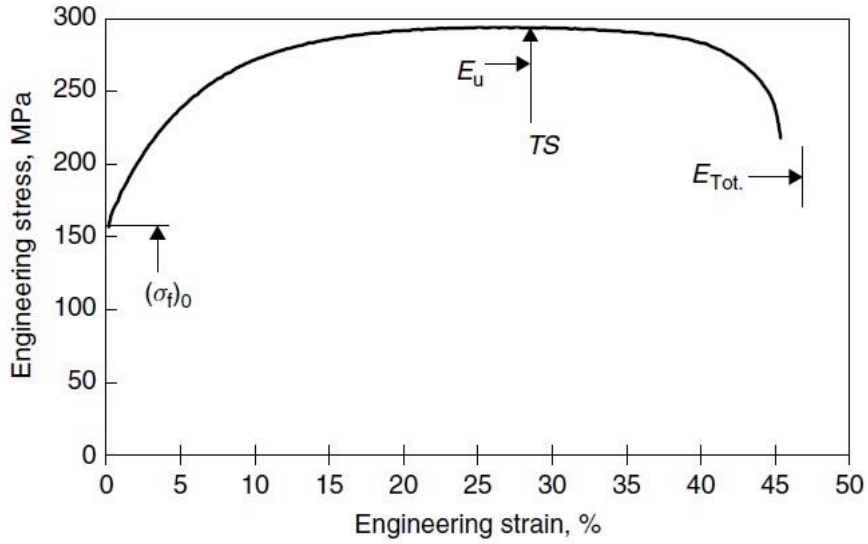

Figure 5.3. Engineering stress–strain curve [50].

This isn't the true stress at max load as the cross-sectional area is no more A_0. The elongation at max load is named the maximum uniform elongation, E_u [50].

If the strain rate close to the origin is greatly growt, the curves elastic part will appear as illustrated in Figure 5.4. The strain at the initial yield, e_y, as noted, is very small, about 0.1%. The elastic part slope of the curve is the elastic modulus also named Young's modulus [50];

$$E = \frac{(\sigma_f)_0}{e_y} \tag{5.6}$$

If the lane is enlarged further than the elastic limit, stable plastic deformation takes place; onto unloading, the elastic strain will be recovered and the unloading line is parallel to the initial elastic loading line. There is a stable plastic strain when the load has been removed as illustrated in Figure 5.4

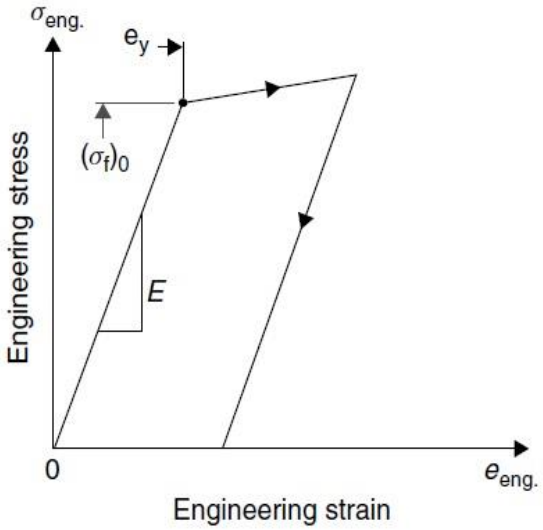

Figure 5.4. The initial part of the elastic strain behavior [50].

In several materials, the transition from elastic to plastic deformation isn't sharp and it is difficult to determine precise yield stress. If this is the case, proof stress may be quoted. This is the stress to cause a specified small plastic strain – often 0.2%, i.e. about twice the elastic strain at yield. The proving stress is established by drawing a line parallel to the elastic loading lane balanced by the specified amount, as illustrated in Figure 5.5

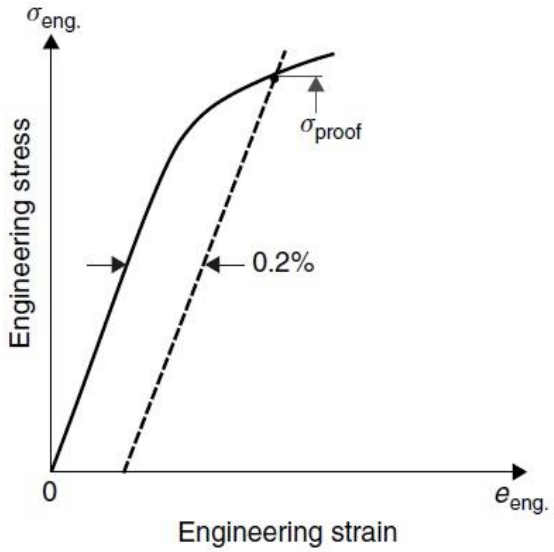

Figure 5.5. Curve applied to define the stress in a material with an elastic, plastic transition [50].

Some steels are delicate to strain aging and will show the phenomenon of yield illustrated in Figure 5.6. This can be in some hot dip galvanized steels and bake hardenable steels used in auto body. Aging has the impact of raising the initial yield stress to the ultimate yield stress σU; further that, flowing takes place discontinuously [50].

In the tensile test piece, discrete rates of deformation will cross the lane under constant tension lower than ultimate yield stress; this is named as the low yield stress σL. Finally of this discontinuous flow, uniform deformation jointed with strain hardening begins. The quantity of discontinuous strain is named yield point elongation (YPE). Steels with a significant YPE of more than about 1% are generally unsuitable for forming as they do not deform properly and visible traces of so-called tensile stresses may appear on the sample [50].

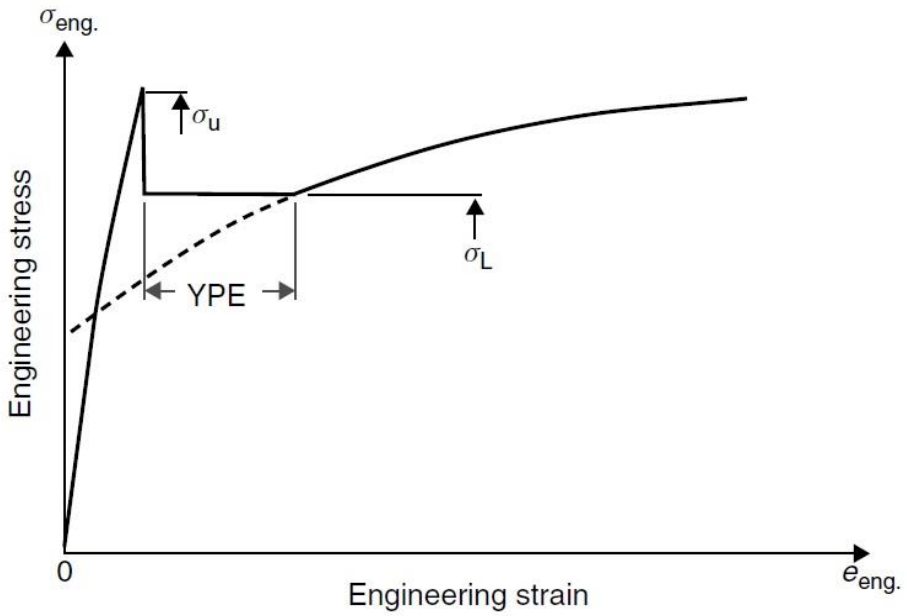

Figure 5.6. YPE on strain aged steel diagram [50].

5.3. THE TRUE STRESS–STRAIN DIAGRAM

There are some reasons why the engineering stress-strain diagram is not suitable for use in the analysis of forming processes.

The concept of stress depends on the initial cross-sectional area of the test sample on the contrary the true value. In addition, since the strain measure is based on the original gauge length, the accuracy of the strain that we will use as engineering is not satisfactory. To overcome these disadvantages, true stress and true strain amounts should be considered when examining forming processes.

True stress;

$$\sigma = \frac{P}{A} \tag{5.7}$$

A is the cross-sectional area. Using the fact that in metals alloys plastic deformation occurs with no appreciable change in volume, the actual stress during the ascending portion of the curve among initial yield and maximum load can be specified from the load-strain graph.

The initial volume and the changing volume are equal;

$$A_0.l_0 = A.l \tag{5.8}$$

True stress is calculated as

$$\sigma = \frac{P.l}{A_0.l_0} \tag{5.9}$$

During test samples deformation, the gauge length grows by a little amount, dl, an appropriate definition of strain is that the strain increase is extension per unit current length.

$$d\varepsilon = \frac{dl}{l} \tag{5.10}$$

For very minor strains, strain increase is the same as engineering strain, but for major strains, there are important differences. If strain continues as in tensile testing uniformly in one direction, strain increase can be integrated to give true strain,

$$\varepsilon = \int d\varepsilon = \int_{l_0}^{l} \frac{dl}{l} = \ln \frac{l}{l_0} \tag{5.11}$$

The true stress-strain graph computed from the load–extension graph above is illustrated in Figure 5.7. Also, this could be computed from the engineering stress-strain graph using the intercourses

$$\sigma = \frac{P}{A} = \frac{P.A_0}{A_0.A} = \sigma_{eng} \frac{l}{l_0} = \sigma_{eng} \left(1 + \frac{e_{eng}}{100}\right) \tag{5.12}$$

in addition

$$\varepsilon = \ln \left(1 + \frac{e_{eng}}{100}\right) \tag{5.13}$$

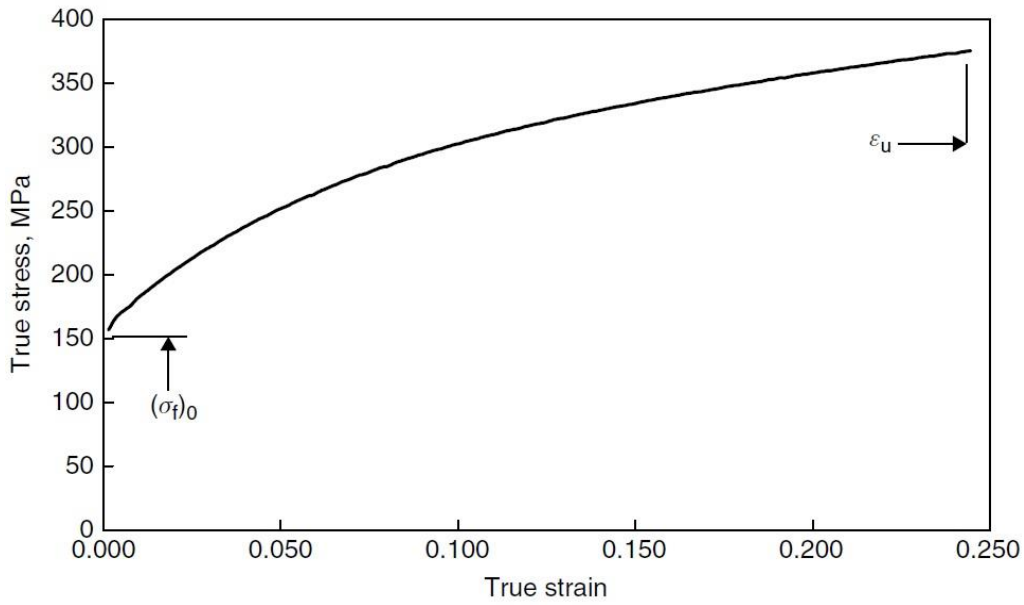

Figure 5.7. The true stress-strain diagram computed from the load–extension graph for sheet steel [50].

This could be seen that the true stress-strain graph doesn't achieve a max strain hardening is continuous though it is formed at a reducing ratio with deformation. When necking begins, deformation in the gauge length isn't any more uniform. Also, Equation 5.11 is no longer valid. The curve in Figure 5.7 cannot be computed outside a strain corresponding to maximum load; this strain is named;

Max uniform strain

$$\varepsilon_u = \ln\left(1 + \frac{E_u}{100}\right) \tag{5.14}$$

If the true stress-strain is plotted on logarithmic values, like in Figure 5.8, many samples of sheets in the soft, annealed status will illustrate the characteristics of this graph. At minor strains in the elastic range, the curve is more or less linear with a slope of unity; this corresponds to an equation for the elastic layout of

$$\sigma = E.\varepsilon \quad \text{or} \quad \log\sigma = logE + log\varepsilon \tag{5.15}$$

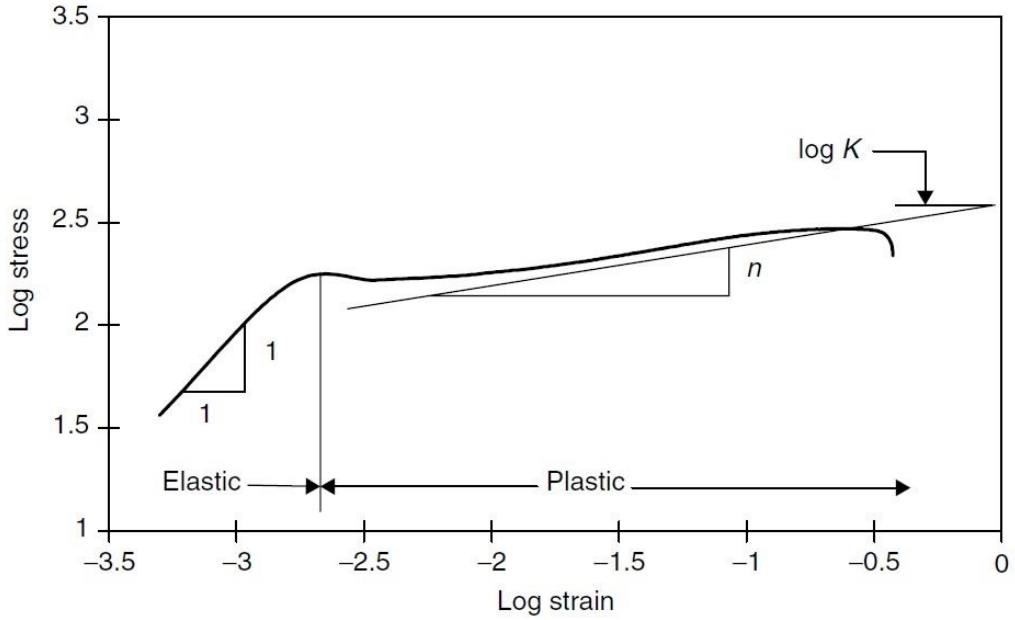

Figure 5.8. The true stress-strain curve plotted in a logarithmic diagram [50].

The curve illustrated can be fitted with an equation of the form at major strains

$$\sigma = K.\varepsilon^n \tag{5.16a}$$

or

$$log\sigma = logK + n.log\varepsilon \tag{5.16b}$$

The illustrated curve has a slope of n, known as the strain hardening index, and an intersection of LogK at unity strain, that is when $\varepsilon = 1$ or $\log \varepsilon = 0$; K is the coefficient of strength. The experimental equation or power-law Equation 5.16a is often used to define the plastic properties of annealed low C sheets. As can be seen from Figure 5.8, it provides an accurate definition except for the first few percentages of the elastic regime and plastic strain. The experimental equations of this form are often used to estimate material property description to stresses greater than those obtainable in tensile testing; this may or may not apply depending on the nature of the material [50].

PART 6

EXPERIMENTAL STUDIES

6.1. OVERVIEW

In this thesis, the chemical content of AISI 316L SS, which is frequently preferred in the medical field, has been determined and it is aimed to experimentally examine the mechanical behaviors that occur as a result of RSW processes. AISI 316L sheet was provided for the test samples to be used in RSW. In this experimental study, experimental pieces were prepared in the light of literature reviews for the welding effects that the test pieces may be exposed to after welding with RSW. Detailed information about these experimental pieces is given in the following sections. In the experimental studies, firstly, the chemical contents of the stainless steel sheet were determined, and then the welding process was carried out with RSW. After the welding process, the nugget sizes in the welded areas and the effects of the welding time on the test samples were examined. In addition, tensile tests were applied to test specimens of two different widths. Experimental data tables were obtained after the experimental investigations. Finally, graphs were created with the obtained tables and many mathematical results were obtained with the graphs created and the formulas used in the tensile test.

6.2. MECHANICAL PROPERTIES OF THE MATERIAL

In order to determine the mechanical properties of the samples to be used before the welding process, to see the tensile diagrams in the computer environment, and to make calculations, samples of two different sizes, A-316L and B-316L, were prepared from AISI 316L SS material. The prepared samples were subjected to a tensile

test in accordance with DIN EN ISO 6892-1 standard. The dimensions of the prepared samples are given in Table 6.1.

Table 6.1. Dimensions of A-316L and B-316L samples.

	Length (mm)	**Width (mm)**	**Thickness (mm)**
A-316L	350	40	1
B-316L	350	30	1

In addition, the samples prepared before the tensile test and the final state of the samples as a result of the tensile test are shown in Figure 6.1 and Figure 6.2.

Figure 6.1. A-316L and B-316L samples prepared before the tensile test.

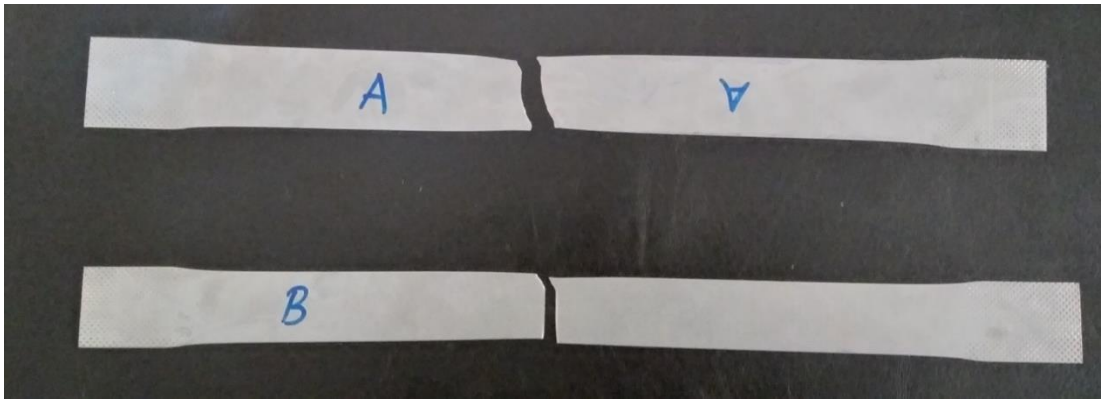

Figure 6.2. A-316L and B-316L samples after tensile test.

The tensile test results on A-316L and B-316L samples were obtained as Excel data and the graphs of the data were created.

The generated engineering stress-strain curves are shown in Figure 6.3 and Figure 6.4.

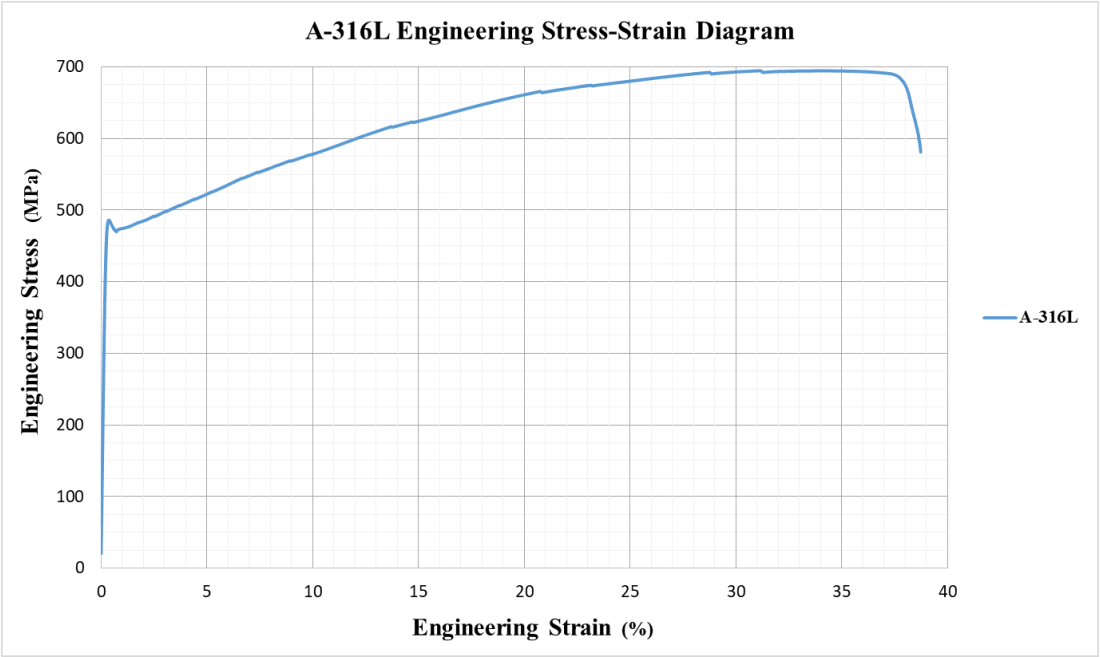

Figure 6.3. A-316L Engineering Stress-Strain diagram.

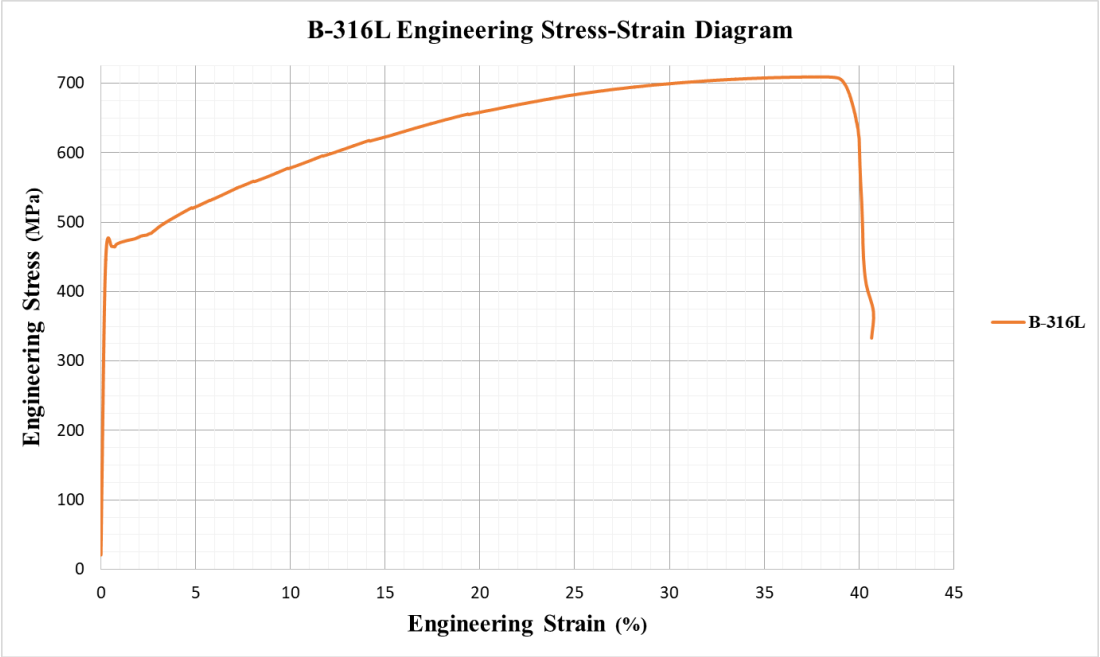

Figure 6.4. B-316L Engineering Stress-Strain diagram.

True Stress-Strain values were found using the engineering stress-strain data obtained as a result of the tensile test and the mathematical operation feature of Excel by writing

a formula. Equation 5.12 and Equation 5.13 is used for this process. In addition, the True Stress-Strain Curves obtained for A-316L and B-316L samples are shown in Figure 6.5 and Figure.6.6.

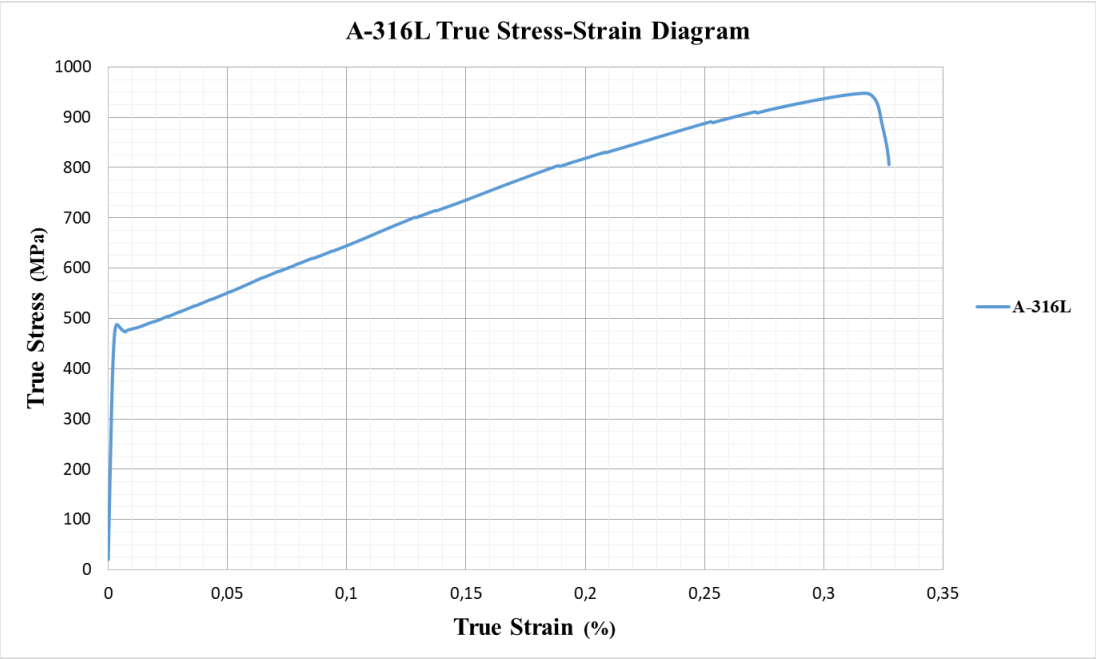

Figure 6.5. A-316L True Stress-Strain diagram.

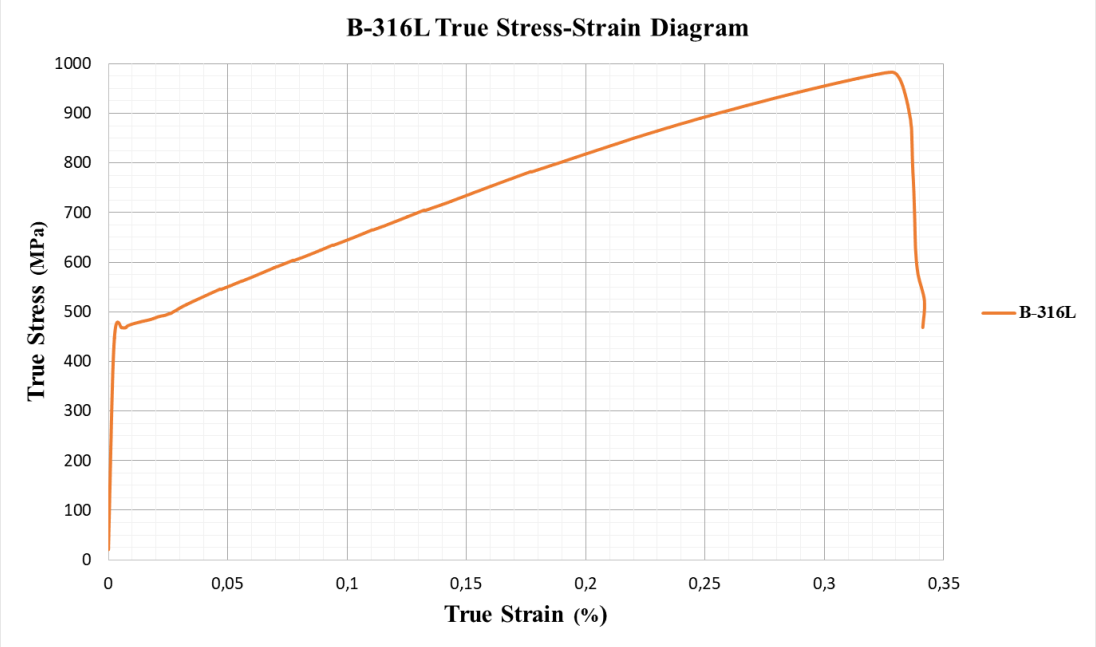

Figure 6.6. B-316L True Stress-Strain diagram.

Logarithmic True Stress-Strain values were found by using the mathematical operation feature of Excel by writing a formula to the real stress-strain values obtained. Equation 5.16b was used in the process. In addition, the Logarithmic True Stress-Strain Curves of the A-316L and B-316L samples are illustrated in Figure 6.7 and Figure 6.8.

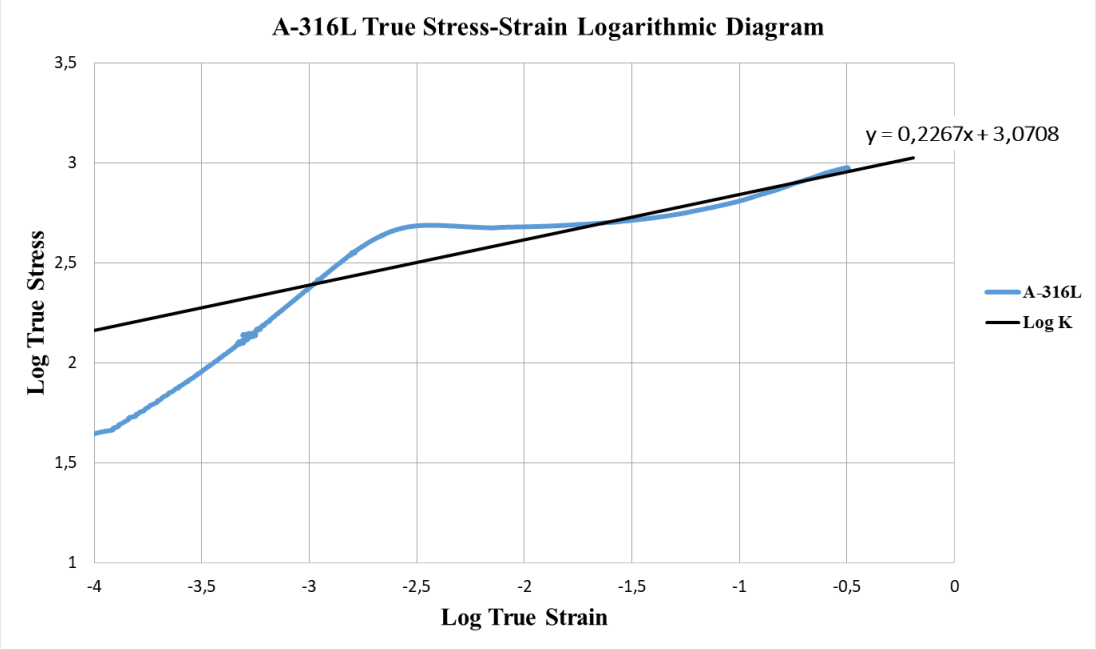

Figure 6.7. A-316L True Stress-Strain Logarithmic diagram

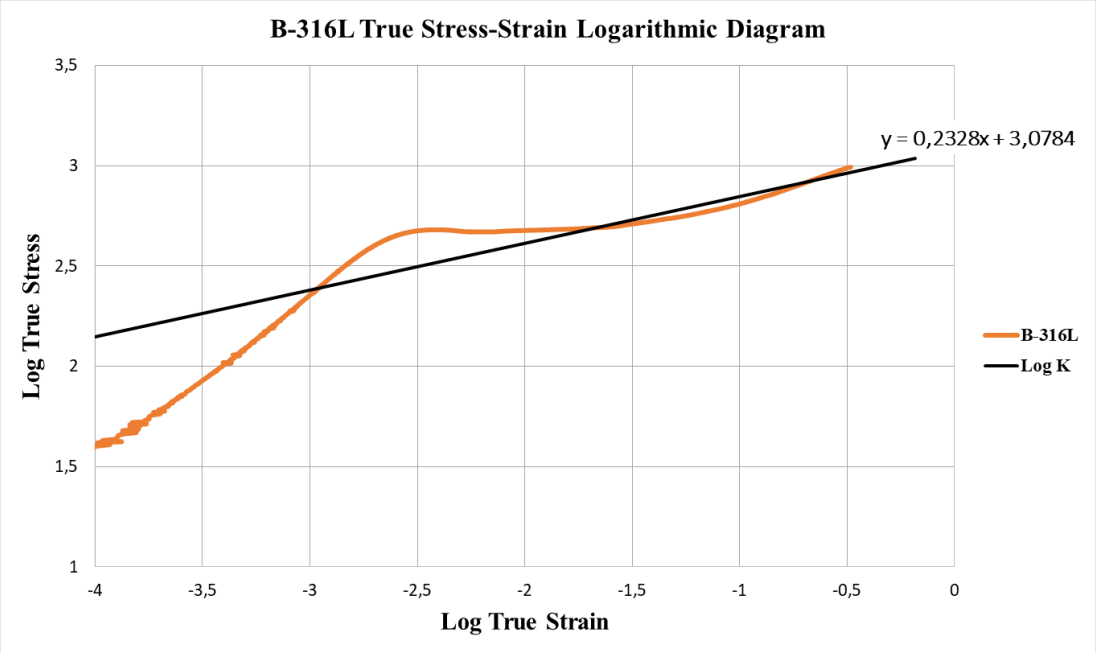

Figure 6.8. B-316L True Stress-Strain Logarithmic diagram.

Log K curves of A-316L and B-316L samples were obtained as a result of the operations performed with Excel.

Mathematical equations to be used, linear equations, and K value are given below.

Linear equation of A-316L sample: y = 0.2267x + 3.0708

When

$x = 0$, $y = logK$

$y = logK = 3.0708$

$10^{log\,K} = 10^{3.0708}$

$K = 1176.5219\,MPa$

Linear equation of B-316L sample: y = 0.2328x + 3.0784

When

$x = 0$, $y = logK$

$y = logK = 3.0784$

$10^{log\,K} = 10^{3.0784}$

$K = 1197.8433\,MPa$

In addition, the mechanical properties obtained from the tensile tests are given in Table 6.2.

Table 6.2. Mechanical properties of A-316L and B316L.

Specimen designation	**$R_{p0.2}$ (MPa)**	**R_{max} (MPa)**	**m_E (GPa)**	**A_{50} (%)**	**K (MPa)**
A-316L	484.1896	694.6252	213.4814	38.46656	1176.5219
B-316L	476.3502	709.1996	206.9369	40.51642	1197.8433

6.3. CHEMICAL ANALYSIS TEST AND CHEMICAL PROPERTIES OF SAMPLES

Metal analysis spectrometer, which is mostly encountered in the chemical industry, is a fast and effective method that enables the chemical structure of metal elements to be distinguished. The purpose of metal analysis spectrometer is to distinguish metal elements both in terms of quality and quantity. This machine is used in the chemical industry and subsidiaries of the chemical industry. The metal analysis spectrometer is considered an ideal choice for applications that require complete disintegration of solid materials. Metal analysis spectrometer analysis utilizes the sparking process, which involves applying an electrical charge to the sample and evaporating low levels of material. It is an ideal method for harder metals and other chemical analysis methods that may be resistant to sparks. Therefore, metal analysis spectrometer was used for the chemical analysis in this study.

In order to perform the chemical analysis test more efficiently and to achieve clearer results, the sample surface must be clean and bright. For this purpose, polishing was applied to the surface of the sample for the chemical test. Stainless steel polishing is the process of polishing the surfaces of stainless steel metals with various surface abrasives. It is a method used for polishing stainless steels and equipment used especially in the health, automotive, furniture, machinery and transportation sectors. It aims to give a bright and flawless appearance with equipment with unwanted abrasive properties such as burrs, scratches, rust on the stainless steel surface, and a smooth appearance is provided on the stainless steel surface. An example of the polishing machine used is given in Figure 6.9

Figure 6.9. An example of the polishing machine used.

The data found as a result of the chemical analyzes are given in Table 6.3.

Table 6.3. Chemical analysis results of AISI 316L SS samples.

Content	**%**	**Temperature (°C)**
C	0.02	22
Si	0. 37	22
S	0.003	22
P	0.028	22
Mn	1.38	22
Ni	10.15	22
Cr	16.85	22
Mo	2.42	22
V	0.10	22
Cu	0.44	22
W	0.06	22
Ti	0.01	22
Nb	0.02	22
Co	0.24	22
Al	0.0	22
N	0.044	22
Fe	Rest	22

6.4. PREPARATION OF TEST SAMPLES

In this study, it was previously stated that experimental studies will be carried out on AISI 316L SS material. Before starting the experimental studies, a sufficient amount of AISI 316L sheet was supplied for the AISI 316L SS samples, which is the main material. The supplied sheet metal is shown in Figure 6.10.

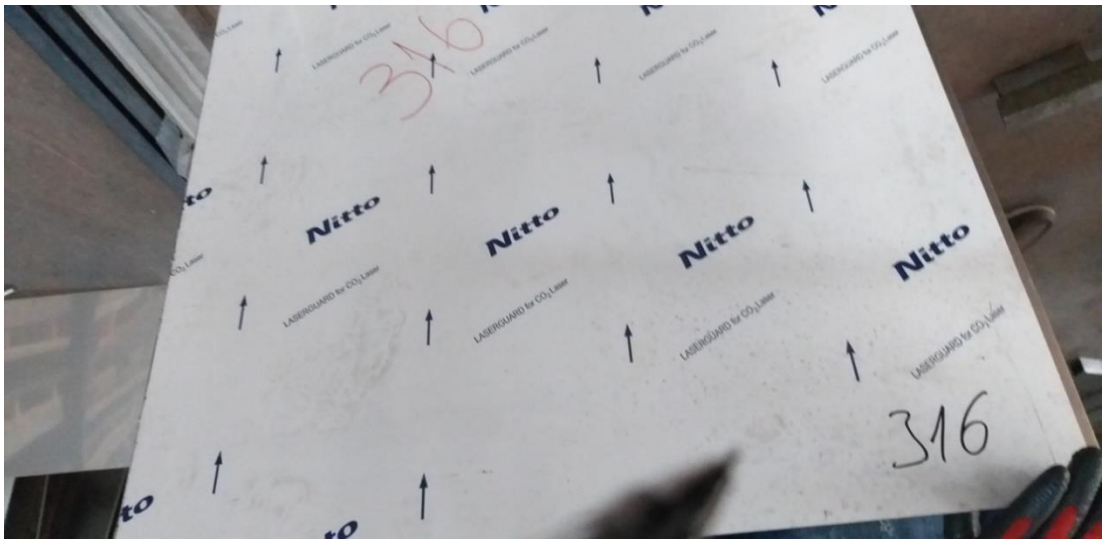

Figure 6.10. The supplied AISI 316L SS sheet metal.

10 welded test specimens will be subjected to tensile testing, so 20 pieces of sheet metal are required for RSW. The parts prepared for the welding process are 350x30x1 mm in size and their dimensions are shown in Figure 6.11.

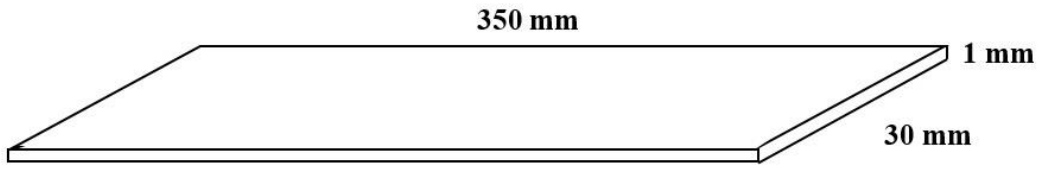

Figure 6.11. Dimensions of AISI 316L SS sheet metal samples.

Sheet metal cutting is a process used to cut metals that are very difficult to cut. We can say that this process is almost the same as the scissors we use in daily life in terms of function. The sheet metal cutting machine has two blades, fixed and movable. The

lower blade is fixed and the upper blade is movable. There is a gap between these blades and this gap varies according to the thickness of the sheet to be cut. The sheet metal cutting machine, which was previously operated by hand, has now left its place in the cutting process with the computer system with the development of technology. In fact, the NC hydraulic sheet metal cutting machine, which is a machine tool, performs cutting by entering the metal data into the system. How and how wide the metal will be cut is added to the computer count management. For this reason, the cutting capacity of sheet metal cutting machines varies a lot. Depending on this change, production measures also change.

In this study, Baykal NC Hydraulic Sheet Metal Cutting Machine was used for metal cutting processes and the metal cutting machine used is shown in Figure 6.12. In addition, the samples obtained after the cutting process are shown in Figure 6.13.

Figure 6.12. Used for metal cutting process Hydraulic Sheet Metal Cutting Machine.

Figure 6.13. AISI 316L sheet metal after the cutting process.

6.5. WELDING PROCESSES WITH RESISTANCE SPOT WELDING

Welding samples were prepared from AISI 316L SS sheet plates with cutting a 350x30x1 mm sheet metal cutting machine. In order to minimize the defects that may occur during welding, the surfaces of the samples to be welded were cleaned. The samples prepared from stainless steel plates were welded with the RSW method in accordance with EN ISO standards. In addition, attention was paid to ensure that the electrodes used were in ISO standards. The RSW and electrodes used during the welding process are shown in Figure 6.14.

Figure 6.14. During the welding process, the resistance spot welding and electrodes.

Welding processes with RSW were carried out at different currents and at different times. The preferred downstream-time process and upstream-time process in the welding process are as in Table 6.4. In addition, the samples that were joined by welding are shown in Figure 6.15.

Table 6.4. Resistance point source lower and upper current-time process control variables;

	Lower	**Upper**
Current (A)	30	50
Time (s)	1	4

Figure 6.15. The samples after the resistance spot welding process.

6.5.1. Current-Time Values Applied to Samples

In order to better observe the mechanical effects of RSW on AISI 316L samples, different current and different duration welding applications were performed. The current and time values used in the implemented application are shown in Table 6.5.

Table 6.5. Current and time values used in welding

Samples No	Current (A)	Time (s)
1	30	1.5
2	30	2
3	30	3
4	40	3
5	40	2
6	40	3.5
7	45	2
8	45	3
9	45	4
10	50	1

6.6. TENSILE TEST OF WELDED SAMPLES

In order to determine the mechanical properties of the RSW processes, a tensile test environment was prepared in accordance with DIN EN ISO 6892-1 standards. This standard covers the tensile test methodology of metallic materials and defines the mechanical properties that can be determined at room temperature. As stated in the standard, tensile tests were carried out by applying an increasing tensile load to 10 test specimens, which were welded with RSW in the prepared test environment, at an ambient temperature of 22 °C. The tensile test setup is shown in Figure 6.16.

Figure 6.16. The experimental setup for tensile testing.

PART 7

EXPERIMENT RESULTS

7.1. MEASUREMENT OF NUGGETS FORMED IN THE RESISTANCE SPOT WELDING PROCESS

It was mentioned that different current and different duration welding applications were carried out in order to better observe the mechanical effects of RSW on AISI 316L samples. The nugget sizes formed as a result of the welding process with RSW at different currents and different time values were measured. An example structure is shown in Figure 6.10 for the nugget formed after RSW. The general scheme of the measurements made is given in Figure 7.1.

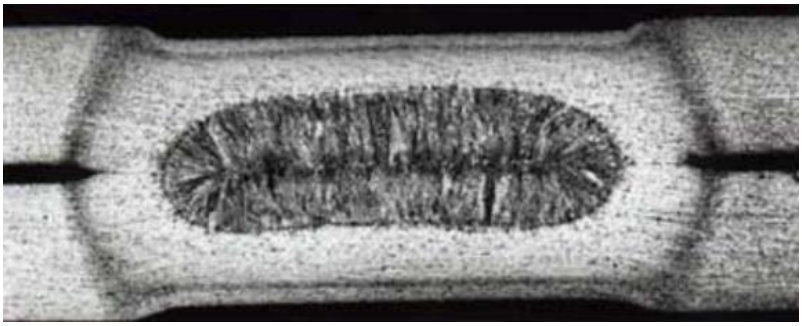

Figure 7.1. Example structure the nugget formed after resistance spot welding [11].

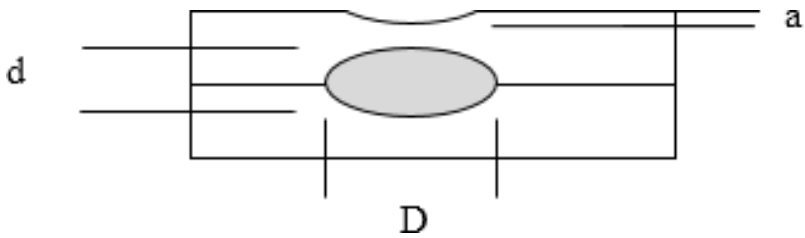

Figure 7.2. The general scheme of the measurements.

Where; a is the electrode penetration depth, d is the nugget height, and D is the nugget width. The results as a result of the measurement procedures are given in Table 7.1.

Table 7.1. Dimensions of nuggets formed by resistance spot welding process.

Sample No	a (mm)	d (mm)	D(mm)
1	0.14	3.42	0.02
2	0.32	4.32	0.14
3	0.48	6.12	0.12
4	0.27	7.0	0.08
5	0.61	6.31	0.11
6	0.70	7.21	0.42
7	0.55	4.34	0.14
8	0.71	6.23	0.21
9	1	7.34	0.01
10	0.21	3.02	0.11

Also, in Table 7.2, the applied different currents and times and nugget measurements are shown in the common table.

Table 7.2. Current-time values and nugget measurements.

Sample No	Current (A)	Time (s)	a (mm)	d (mm)	D (mm)
1	30	1.5	0.14	3.42	0.02
2	30	2	0.32	4.32	0.14
3	30	3	0.48	6.12	0.12
4	40	3	0.27	7.0	0.08
5	40	2	0.61	6.31	0.11
6	40	3.5	0.70	7.21	0.42
7	45	2	0.55	4.34	0.14
8	45	3	0.71	6.23	0.21
9	45	4	1	7.34	0.01
10	50	1	0.21	3.02	0.11

There are serious differences in the nugget sizes that occur as a result of RSW and welding processes at different current values and different times. Before comparing the nugget size differences at different currents and times, it is necessary to look at the welding processes with RSW at the same current value at different times.

In the previous section, the current and time values applied to the samples were given to compare the nugget sizes. As it will be remembered, the application of 30A current value was made to samples 1, 2 and 3, and the processing time was kept for 1.5 - 2 - 3 seconds, respectively. Another applied current value, 40A, has been applied to samples 4, 5 and 6, and welding times are 3 – 2 – 3.5 seconds, respectively. The other current value, 45A, to be used in the comparison of nugget sizes, was made on samples 7, 8 and 9, and the processing time is 2 – 3 – 4 seconds, respectively. In addition, 50A current value was applied to sample 10 for 1 second. As a result of the applications, nugget size changes will be compared. As it is known, welding current and welding time are the main factors affecting nugget sizes. This is because an increase in any of the current or time parameters will significantly increase the heat accumulation on the sample. Welding current, welding time and heat build-up form the basis for comparisons. Comparisons to be made with the data obtained will be for the electrode penetration depth and nugget width, which are the factors that affect the mechanical properties the most. When comparing nugget sizes, dividing the samples into 3 groups as 30A, 40A and 45A according to the same current values will facilitate the comparisons.

Firstly, electrode penetration depth and nugget widths that occur after the welding process in samples 1,2 and 3, where 30A current value is applied, will be given respectively. While the electrode penetration depth in sample 1 was 0.14 mm, the nugget width was measured 0.02 mm. While the electrode penetration depth in sample 2 was 0.32 mm, the nugget width was measured 0.14 mm. In sample 3, the electrode penetration depth was 0.48 mm, while the nugget width was 0.12 mm. While heat accumulation, which is one of the leading factors affecting nugget sizes, did not occur in sample 1, heat accumulation in samples 2 and 3 was more due to longer welding times. In samples 2 and 3, heat accumulation occurred, albeit in a small amount, and the nugget size was higher than the nugget size formed in sample 1. In this comparison

group, the effects of duration in RSW were generally seen for nugget width. In addition, Figure 7.3 shows the variation of nugget sizes with 30A current value with time.

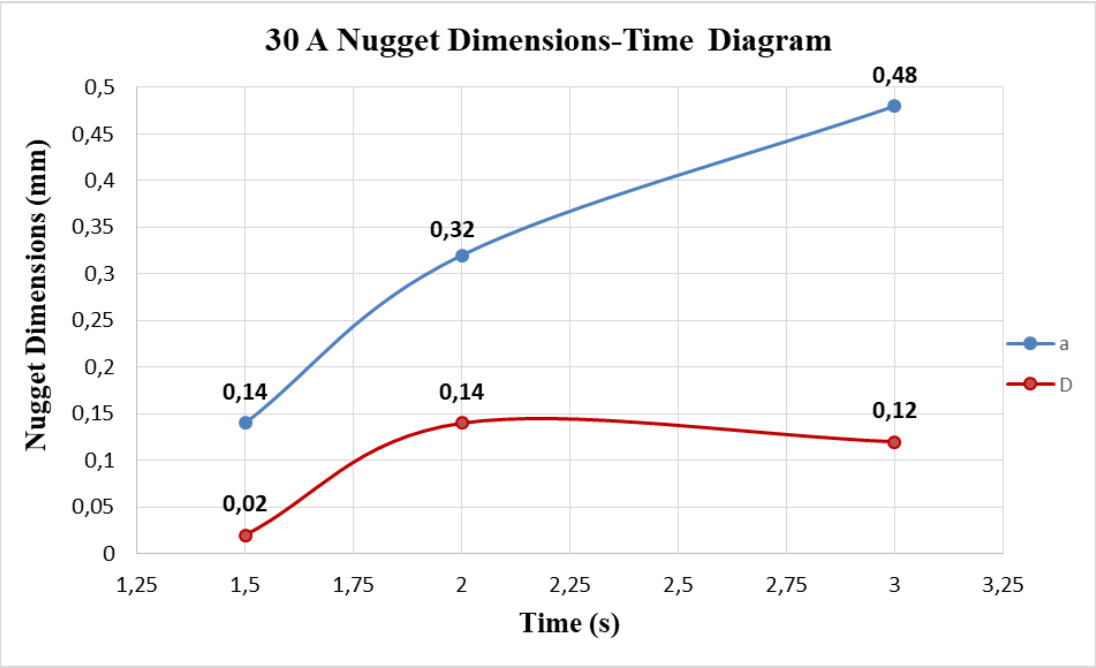

Figure 7.3. 30 A Nugget Dimensions-Time diagram.

Secondly, if we look at the samples numbered 4.5 and 6, where 40A current value is applied, the nugget dimensions that occur after the welding process will be given respectively. While the electrode penetration depth in sample 4 was 0.27 mm, the nugget width was measured 0.08 mm. While the electrode penetration depth in sample 5 was 0.61 mm, the nugget width was 0.11 mm. In sample 6, the electrode penetration depth was 0.70 mm, while the nugget width was 0.42 mm. Contrary to the previous comparison group, the amount of heat accumulation in samples 4 and 5 was less than in sample 6 this time. This may not be enough to explain the high difference in nugget sizes. So the nugget height should also be looked at. When the samples are examined respectively, it is seen that the nugget heights increase from the one with less welding time to the one with more. Therefore, in the comparison made for this group, it has been seen that while the nugget height value increases normally during nugget formation, fluctuations may occur in other parameters. In addition, Figure 7.4 shows the variation of nugget sizes with time at the 40A current value.

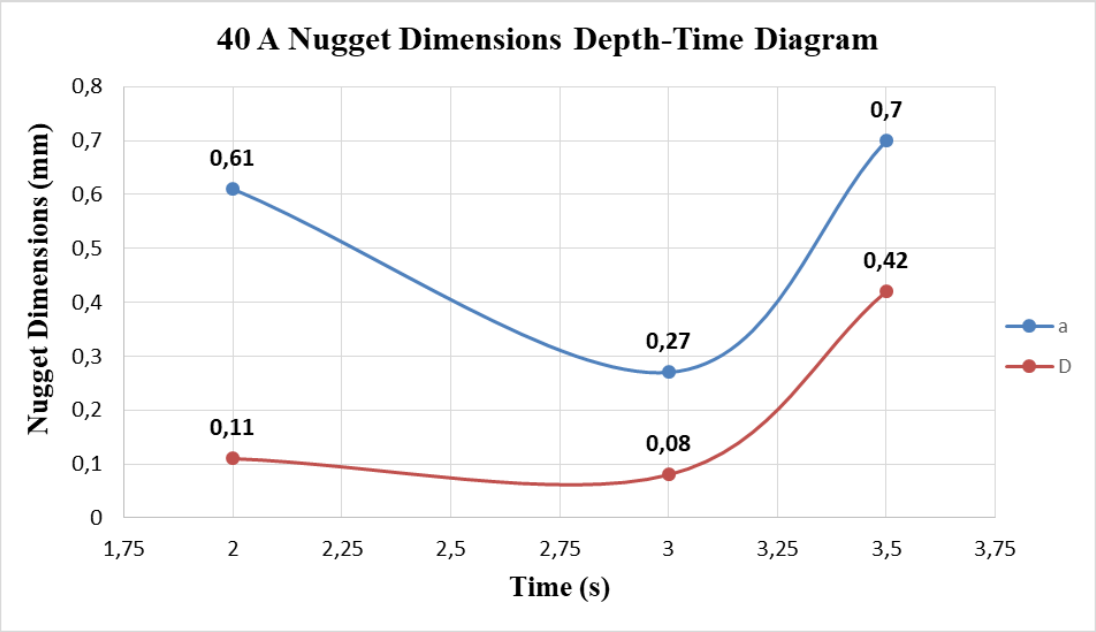

Figure 7.4. 40 A Nugget Dimensions-Time diagram.

Finally, if we look at the samples numbered 7,8 and 9, on which the current value of 45A is applied, the nugget dimensions that occur after the welding process are given respectively. While the electrode penetration depth in sample 7 was 0.55 mm, the nugget width was 0.14 mm. While the electrode penetration depth in sample 8 was 0.71 mm, the nugget width was measured as 0.21 mm. In sample 9, while the electrode penetration depth was 1.00 mm, the nugget width was measured as 0.01 mm. This comparison group has enabled us to fully see the effects of welding current and welding time on the samples compared to others. When looking at sample number 9, the nugget formed as a result of heat accumulation was formed around the points to be welded. Therefore, these data showed the importance of welding current and welding time in the welding process with RSW. In addition, Figure 7.5 illustrated the variation of nugget sizes with time at 45A current value.

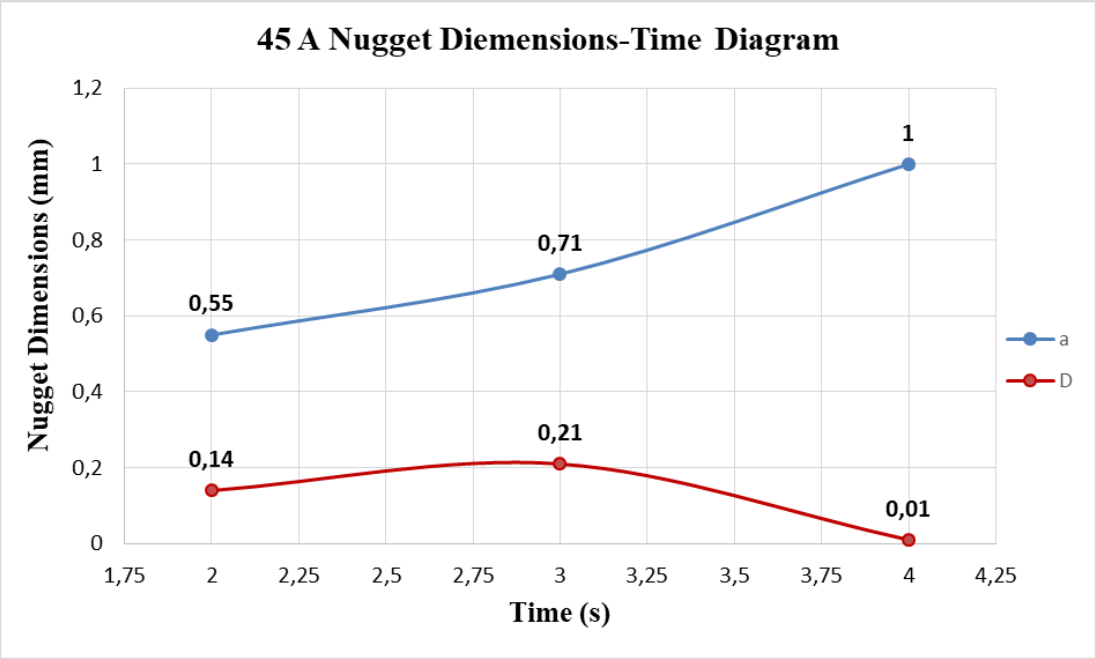

Figure 7.5. 45 A Nugget Dimensions-Time diagram.

In this section, the effects of applied welding current and welding times are compared. As a result of the comparisons, the importance of current and time for the welding process is emphasized. Optimum current and time values will be determined for this study by comparing the results of the tensile tests performed on the samples. In addition, in Figure 7.6, Figure 7.7 and Figure 7.8, measurement variation graphs of the groups compared with the same parameters are given. These graphs were added to see the effects of current and time parameters on electrode penetration depth, nugget height and nugget width values used in nugget measurements from different angles.

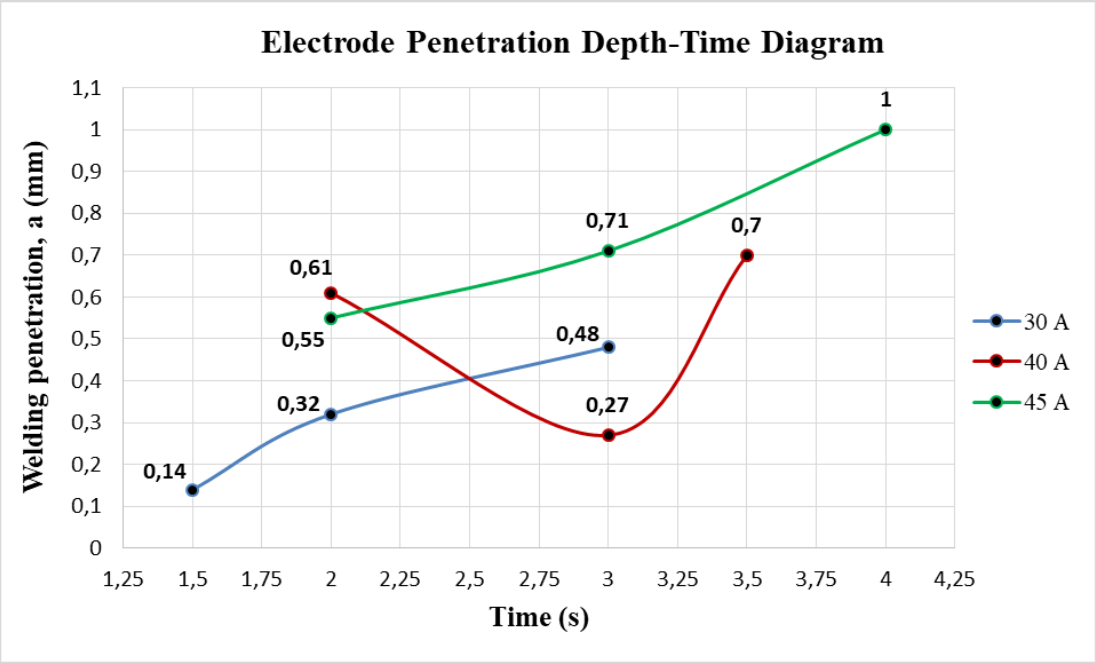

Figure 7.6. Electrode Penetration Depth-Time diagram.

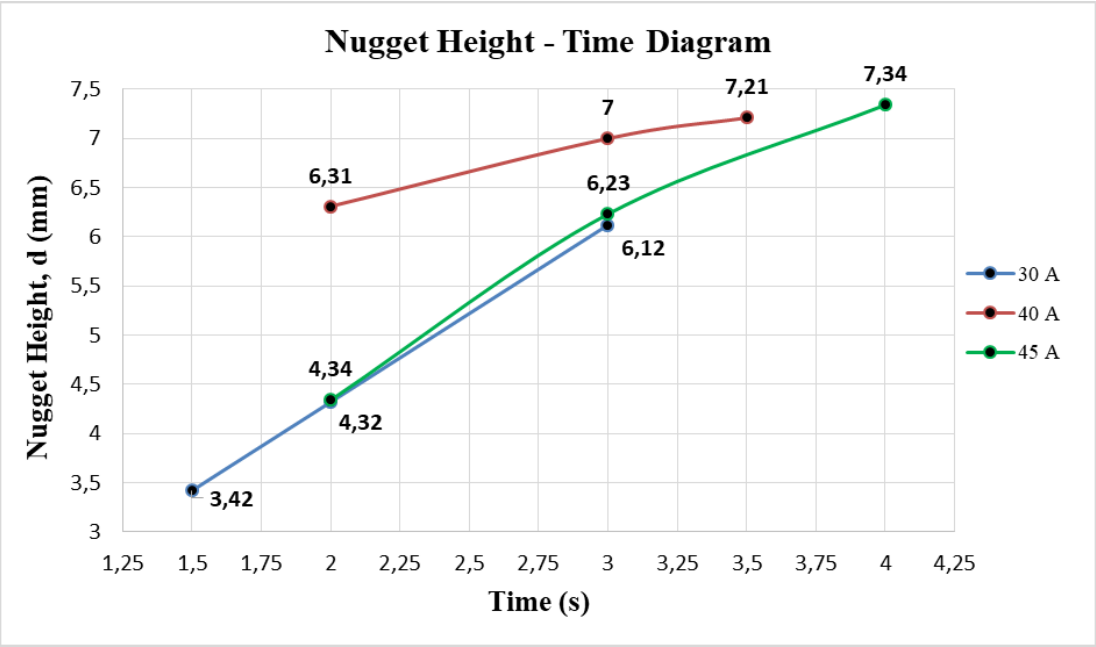

Figure 7.7. Nugget Height-Time diagram.

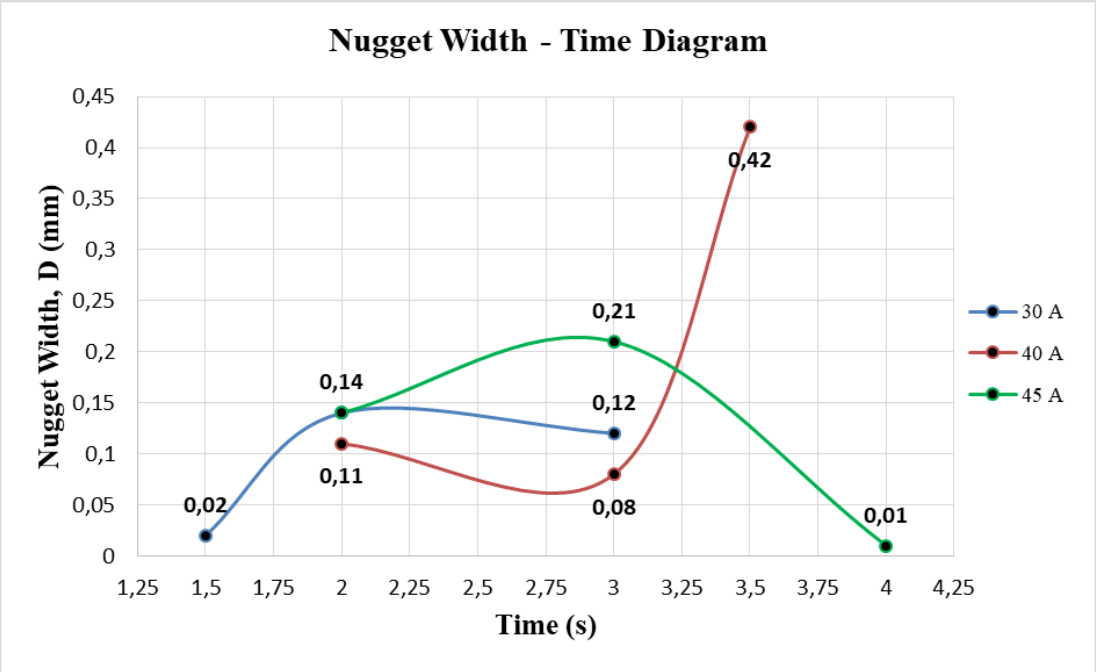

Figure 7.8. Nugget Width-Time diagram.

7.2. TENSILE TEST RESULTS

To determine the mechanical properties of RSW processes applied to AISI 316L samples, a tensile test environment was prepared by DIN EN ISO 6892-1 standards. The tensile test results are given in Table 7.3. In addition, the current-time-load table is given in Table 7.4.

Table 7.3. Maximum load table obtained as a result of the tensile test applied at 22ºC.

Sample No	Maximum load (kN)	Temreture (ºC)
1	11.24	22
2	14.74	22
3	18.70	22
4	18.26	22
5	20.60	22
6	23.02	22
7	19.88	22
8	17.86	22
9	17.48	22
10	14.44	22

Table 7.4. Maximum load table obtained as a result of the tensile test applied at 22ºC

Sample No	**Current (A)**	**Time (s)**	**Maximum load (kN)**
1	30	1.5	11.24
2	30	2	14.74
3	30	3	18.70
4	40	3	18.26
5	40	2	20.60
6	40	3.5	23.02
7	45	2	19.88
8	45	3	17.86
9	45	4	17.48
10	50	1	14.44

It is always more appropriate to use mathematical approximation methods to logically compare the maximum load values obtained from the analyzes. Therefore, the graph of the applied welding current values with the maximum load obtained from the tensile tests was created. In addition, the parabolic regression method, one of the mathematical approach methods, was used. The reason for this is that although some engineering data have a certain shape, it may not be possible to represent the obtained data with a straight line. In such cases, a parabolic curve may be more fitting to the data, and fitting a polynomial curve may yield more accurate results. Since the data obtained from the tensile tests also fit this situation, the curve fitting method was polynomial, that is, parabolic.

The graph showing the regression curve created with the maximum load and source current value data is shown in Figure 7.9. In addition, the result of the mathematical approach, R^2 value was 0.5853.

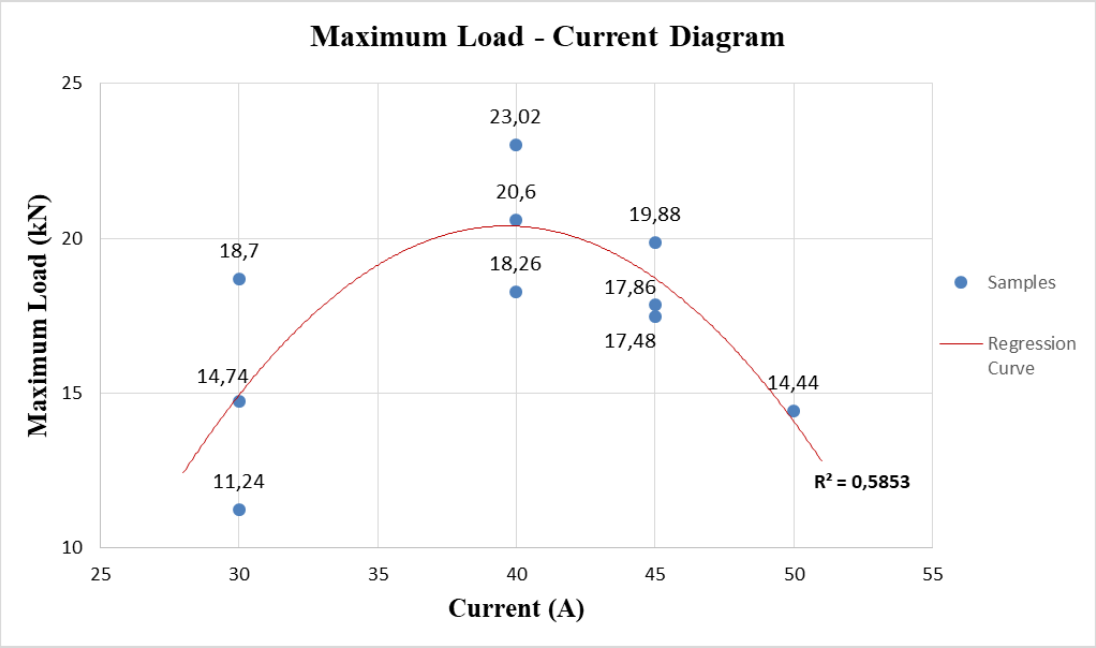

Figure 7.9. Maximum Load-Current regression diagram.

As a result of curve fitting with the regression method, the values above the regression curve are acceptable values as a result of the tensile test. It would be more accurate to explain this situation by grouping it according to the source current values.

Of the maximum load values of samples 1, 2 and 3, where the first value of 30A welding current value is applied, only the maximum load value of sample 3 remains above the regression curve. Therefore, while it can be said that the welding process with RSW on sample 3 is sufficient and safe, it cannot be said for the welding process on samples 1 and 2.

The maximum load values of samples 5 and 6 of samples 4, 5 and 6, to which the second value, 40A welding current value, are applied, are above the regression curve. Therefore, it can be said that welding with resistance spot welding on samples 5 and 6 is sufficient and safe, but the welding on sample 4 is not sufficient.

Of the maximum load values of samples 7, 8 and 9, to which the third value, 45A welding current value, is applied, only the maximum load value of sample number 7 remains above the regression curve. Therefore, it can be said that welding with RSW on sample 7 is sufficient and safe, but it cannot be said for welding on samples 8 and

9. Finally, the maximum load value of sample 10, to which 50A welding current value is applied, remains above the regression curve. Therefore, it can be said that welding at 50A current and 1 second is sufficient and safe. The final state of the whole tensile testing samples is given in Figure 7.10.

Figure 7.10. The final state of the tensile testing samples.

PART 8

RESULTS

8.1. SUMMARY OF THE STUDY

In this study, the welding effects and mechanical properties of AISI 316L SS sheet plates, which are widely used in medical fields, after RSW were experimentally analyzed. Many literatures have been examined in order to have an idea for the studies to be done and the information obtained from this literature has been added to the study as a summary. The study was first started by determining the mechanical properties of AISI 316L SS material. For this, firstly, A-316L and B-316L samples were prepared. The samples dimensions are 350x40x1 mm and 350x30x1 mm, respectively. The tensile test was applied to the prepared samples and the data obtained were recorded as Excel tables. The obtained data were then calculated using the Engineering Stress-Strain, True Stress-Strain and Logarithmic True Stress-Strain formulas. Tensile test formulas were used in the calculations. The data obtained as a result of the calculations were converted into Excel graphics. The Log K value was obtained with the help of the Logarithmic True Stress-Strain curve from the generated graphics. As a result of the processes, the K value of the A-316L sample was found to be 1176.52 MPa, while the K value of the B-316L sample was found to be 1197.84 MPa.

After determining the mechanical properties of the material to be used in the study, chemical analysis was performed on the sample taken from the material with a Metal Analysis Spectrometer in order to determine its chemical structure. Before chemical analysis, polishing was done to eliminate surface defects. The chemical structure of the AISI 316L material obtained as a result of the chemical analysis is given in the table.

After the material properties were determined, the sample preparation stage was started for the RSW process. Since 20 samples of 350x30x1 mm in size will be needed for the welding process, AISI 316L SS plate with dimensions sufficient for the samples was taken. Since the received AISI 316L sheet metal is a high-strength material, Sheet Metal Cutting Machine was used to prepare the sample. After the samples were prepared, the welding process was started. 20 samples prepared at this stage were welded with RSW. In this study, since the mechanical effects of welding with RSW will be examined, the samples were welded at different current values and different time parameters. After welding, a total of 10 samples were prepared. While welding current values of 30A, 40A, 45A and 50A were used in the welding process, welding times were kept within the range of 1 to 4 seconds. In addition, the nuggets formed after welding were examined in order to form an idea while examining the effect of welding on mechanical effects at different current and time parameters. As a result of the examinations, nugget formation was at a low level in sample 1 using 30A - 1.5s welding parameters. On the contrary, the surface of the sheet metal was completely deformed after the welding process applied in sample 9 using 45A – 4s welding parameters.

After the operations and comparisons, the last operation, the tensile test, was started. In this process, the maximum load was applied to the welded 10 samples and the rupture of the welding areas was ensured. In addition, the tensile test data were saved as Excel data. A common table was created by combining the recorded data with other data. In order to compare the data obtained as a result of the tensile test, the Maximum Load-Current graph was created and in order to apply a mathematical approach to this graph, polynomial regression, which is one of the curve fitting methods, was applied. In the applied polynomial regression process, a parabolic curve was formed on the graph and the R^2 value of this curve was found to be 0.5853. With the mathematical approach, it was determined that the samples with sufficient and reliable mechanical properties were samples 3, 5, 6, 7 and 10. In addition, after the comparison, it was determined that the first three samples with the highest maximum load were samples 5, 6 and 7. In addition, the sample with the highest maximum load was sample 6 with a value of 23.02 kN. Therefore, it has been concluded that the optimum welding

current is 40A and the welding time is 3.5s after the RSW process. The image of sample number 6 after the tensile test is given in Figure 8.1

Figure 8.1. The image of sample number 6 after the tensile test.

In addition, nugget measurements and maximum load values after welding are shown in Table 8.1 as a common table.

Table 8.1. Nugget measurements and maximum load values after welding operations and tensile tests.

Sample No	**Current (A)**	**Time (s)**	**a (mm)**	**d (mm)**	**D (mm)**	**Maximum load (kN)**
1	30	1.5	0.14	3.42	0.02	11.24
2	30	2	0.32	4.32	0.14	14.74
3	30	3	0.48	6.12	0.12	18.70
4	40	3	0.27	7.0	0.08	18.26
5	40	2	0.61	6.31	0.11	20.60
6	40	3.5	0.70	7.21	0.42	23.02
7	45	2	0.55	4.34	0.14	19.88
8	45	3	0.71	6.23	0.21	17.86
9	45	4	1	7.34	0.01	17.48
10	50	1	0.21	3.02	0.11	14.44

8.2. CONCLUSION

In this study, an experimental investigation of AISI 316L SS, which is frequently preferred in medical fields, has been made. As a result of the studies and tensile test data obtained, it was concluded that the material is at a level that can meet most effects in daily life as a result of the application of RSW on AISI 316L.

In addition, the results obtained after the experimental studies are as follows;

a. While the heat build-up in the samples with 30A welding current did not occur in the 1st sample, the heat build-up in the 2nd and 3rd samples was more due to the longer welding times. In samples 2 and 3, heat accumulation occurred, albeit in a small amount, and the nugget size was higher than the nugget size formed in sample 1. In addition, as a result of the tensile tests, it can be said that the welding process with RSW on sample 3 is sufficient and safe, but it cannot be said for the welding process on samples 1 and 2.
b. The maximum load value for samples with a welding current of 30A is 18.70 kN.
c. The amount of heat condensation occurring in the samples applied with 40A welding current in samples 4 and 5 was less than in sample 6. In addition, as a result of the tensile tests, it can be said that the resistance spot welding performed on samples 5 and 6 is sufficient and safe, while the welding process on sample 4 is not sufficient.
d. The maximum load value for samples with a welding current of 40A is 23.02 kN.
e. The nugget, which was formed as a result of heat accumulation in sample 9 of the samples applied with a welding current of 45A, was formed around the points to be welded. This comparison group has enabled us to fully see the effects of welding current and welding time on the samples compared to others. In addition, as a result of the tensile tests, it can be said that the welding process with resistance spot welding on sample 7 is sufficient and safe, but it cannot be said for the welding process on samples 8 and 9.

f. The maximum load value for samples with a welding current of 45A is 19.88 kN.
g. Comparisons made after welding showed the importance of welding current and welding time in welding with resistance spot welding.
h. After the tensile test, the maximum load value of sample 10 remains above the regression curve. Therefore, it can be said that welding at 50A current and 1 second is sufficient and safe. The maximum load obtained after welding is 14.44 kN. Although this value is thought to be not sufficient at first glance, it indicates that the nugget sizes that will occur as a result of high welding current and low welding time may be close to the optimum value.
i. As a result of the experiments and comparisons, it was concluded that the optimum values were the values of welding current 40A and welding time 3.5s in sample 6.

8.3. SUGGESTIONS

As everyone knows, no experimental work goes perfectly. Therefore, it may be necessary to share the knowledge experienced during experimental studies. The knowledge gained after this study will be presented as suggestions.

a. If the AISI 316L samples prepared for experimental studies can be prepared exactly with standard values, the mechanical properties to be obtained can be more accurate.
b. The more stable operation of the resistance spot welding system used for the welding process increases the welding quality and more clear data can be obtained in experimental comparisons.
c. The welding process will increase the reality of the data to be obtained by autonomous welding systems instead of manpower.
d. Care must be taken to ensure that the pressure to be applied during the welding process is at more stable values. Otherwise, the desired nugget sizes cannot be obtained in the specified parameters.
e. The most important point to be considered in experimental studies on welding processes is that the welding processes are applied in a standard way.

Otherwise, there may be differences in the nugget sizes formed, and the desired nugget sizes may not be reached. Therefore, these effects will also affect the results obtained from the tensile tests.

REFERENCES

1. Talha, M., Behera, C. K., & Sinha, O. P., "A review on nickel-free nitrogen containing austenitic stainless steels for biomedical applications." ***Materials Science and Engineering:*** *C*, *33*(7), 3563-3575 (2013).

2. Sumita, M., Hanawa, T., & Teoh, S. H., "Development of nitrogen-containing nickel-free austenitic stainless steels for metallic biomaterials." ***Materials Science and Engineering****: C*, *24*(6-8), 753-760 (2004).

3. Sumita, M., Ikada, Y., & Tateishi, T., "Metallic Biomaterials-Fundamentals and Applications." ***ICP***, *Tokyo*, 629 (2000).

4. Marashi, P., Pouranvari, M., Amirabdollahian, S., Abedi, A., & Goodarzi, M., "Microstructure and failure behavior of dissimilar resistance spot welds between low carbon galvanized and austenitic stainless steels." ***Materials science and engineering****: A*, *480*(1-2), 175-180 (2008).

5. Verma, A. B., Ghunage, S. U., & Ahuja, B. B., "Resistance Welding of Austenitic Stainless Steels (AISI 304 with AISI 316)." In ***5th International & 26th All India Manufacturing Technology, Design and Research Conference (AIMTDR 2014) IIT Guwahati***, *Assam, India* (2014, December).

6. Shelly, K., & Sahota, D. S., "A Review Paper on Resistance Spot Welding of Austenitic Stainless Steel 316." (2017).

7. Mohammed, H. G., Ginta, T. L., & Mustapha, M., "The investigation of microstructure and mechanical properties of resistance spot welded AISI 316L austenitic stainless steel." ***Materials Today: Proceedings***, *46*, 1640-1644 (2021).

8. Khuenkaew, T., & Kanlayasiri, K., "Optimizing the resistance spot-welding process for dissimilar stainless steels." In ***IOP Conference Series: Materials Science and Engineering*** (Vol. 361, No. 1, p. 012005). IOP Publishing (2018, May).

9. Fukumoto, S., Fujiwara, K., Toji, S., & Yamamoto, A., "Small-scale resistance spot welding of austenitic stainless steels." ***Materials Science and Engineering:*** *A*, *492*(1-2), 243-249 (2008).

10. Pouranvari, M., Alizadeh-Sh, M., & Marashi, S. P. H., "Welding metallurgy of stainless steels during resistance spot welding Part I: fusion zone." ***Science and Technology of Welding and Joining***, *20*(6), 502-511 (2015).

11. Alizadeh-Sh, M., Pouranvari, M., & Marashi, S. P. H., "Welding metallurgy of stainless steels during resistance spot welding part II–heat affected zone and mechanical performance." ***Science and Technology of Welding and Joining***, *20*(6), 512-521 (2015).

12. Moshayedi, H., & Sattari-Far, I., "Numerical and experimental study of nugget size growth in resistance spot welding of austenitic stainless steels." ***Journal of Materials Processing Technology***, *212*(2), 347-354 (2012).

13. Jamaludin, S. B., Hisyam, M. M., Shamsudin, S. R., Darus, M., & Wahid, M. F. M., "Study of spot welding of austenitic stainless steel type 304." (2007).

14. Arabi, S. H., Pouranvari, M., & Movahedi, M., "Pathways to improve the austenite–ferrite phase balance during resistance spot welding of duplex stainless steels." ***Science and technology of welding and joining***, *24*(1), 8-15 (2019).

15. Moteshakker, A., Danaee, I., Moeinifar, S., & Ashrafi, A., "Hardness and tensile properties of dissimilar welds joints between SAF 2205 and AISI 316L." ***Science and Technology of Welding and Joining***, *21*(1), 1-10 (2016).

16. Eşme, U., "APPLICATION OF TAGUCHI METHOD FOR THE OPTIMIZATION OF RESISTANCE SPOT WELDING PROCESS." ***Arabian Journal for Science & Engineering (Springer Science & Business Media BV),*** *34* (2009).

17. Bekmurzayeva, A., Duncanson, W. J., Azevedo, H. S., & Kanayeva, D., "Surface modification of stainless steel for biomedical applications: Revisiting a century-old material." ***Materials Science and Engineering: C***, *93*, 1073-1089 (2018).

18. Dewidar, M. M., Khalil, K. A., & Lim, J. K., " Processing and mechanical properties of porous 316L stainless steel for biomedical applications." ***Transactions of Nonferrous Metals Society of China***, *17*(3), 468-473 (2007).

19. Bandar, A. M., Mongrain, R., Irissou, E., & Yue, S., "Improving the strength and corrosion resistance of 316L stainless steel for biomedical applications using cold spray." ***Surface and Coatings Technology***, *216*, 297-307 (2013).

20. Shih, C. C., Shih, C. M., Su, Y. Y., Su, L. H. J., Chang, M. S., & Lin, S. J., "Effect of surface oxide properties on corrosion resistance of 316L stainless steel for biomedical applications." ***Corrosion Science***, *46*(2), 427-441 (2004).

21. Amanov, A., Lee, S. W., & Pyun, Y. S., "Low friction and high strength of 316L stainless steel tubing for biomedical applications." ***Materials Science and Engineering****: C*, *71*, 176-185 (2017).

22. Barros, S. E., Vanz, V., Chiqueto, K., Janson, G., & Ferreira, E., "Mechanical strength of stainless steel and titanium alloy mini-implants with different diameters: an experimental laboratory study." ***Progress in Orthodontics,*** *22*(1), 1-9 (2021).

23. Amalraju, D., & Dawood, A. S., "Mechanical strength evaluation analysis of stainless steel and titanium locking plate for femur bone fracture." ***Engineering Science and Technology: An International Journal***, *2*(3), 381-388 (2012).

24. Hansen, D. C., "Metal corrosion in the human body: the ultimate bio-corrosion scenario." ***The Electrochemical Society Interface***, *17*(2), 31 (2008).

25. Geanta, V., Voiculescu, I., Stefanoiu, R., & Rusu, E. R., "Stainless steels with biocompatible properties for medical devices." In ***Key Engineering Materials*** (Vol. 583, pp. 9-15). Trans Tech Publications Ltd (2014).

26. Kianersi, D., Mostafaei, A., & Amadeh, A. A., "Resistance spot welding joints of AISI 316L austenitic stainless steel sheets: Phase transformations, mechanical properties and microstructure characterizations." ***Materials & Design***, *61*, 251-263 (2014).

27. Kianersi, D., Mostafaei, A., & Mohammadi, J., "Effect of welding current and time on the microstructure, mechanical characterizations, and fracture studies of resistance spot welding joints of AISI 316L austenitic stainless steel." ***Metallurgical and Materials Transactions*** *A*, *45*(10), 4423-4442 (2014).

28. Mansor, M. S. M., Yusof, F., Ariga, T., & Miyashita, Y., "Microstructure and mechanical properties of micro-resistance spot welding between stainless steel 316L and Ti-6Al-4V." ***International Journal of Advanced Manufacturing Technology***, *96* (2018).

29. Vigneshkumar, M., Varthanan, P. A., & Raj, Y. M. A., "Finite element-based parametric studies of nugget diameter and temperature distribution in the resistance spot welding of AISI 304 and AISI 316L sheets." ***Transactions of the Indian Institute of Metals***, *72*(2), 429-438 (2019).

30. Capus, J., "100 Years of Stainless Steel." ***Metal Powder Report***, *68*(5), 12 (2013).

31. McGuire, M. F., "Stainless steels for design engineers." ***Asm International*** (2008).

32. Lula, R. A., "Stainless steel." (1985).

33. Lo, K. H., Shek, C. H., & Lai, J. K. L., "Recent developments in stainless steels." ***Materials Science and Engineering****: R: Reports*, *65*(4-6), 39-104 (2009).

34. Sumita, M., Hanawa, T., & Teoh, S. H., "Development of nitrogen-containing nickel-free austenitic stainless steels for metallic biomaterials." ***Materials Science and Engineering****: C*, *24*(6-8), 753-760 (2004).

35. Mathiesen, T., & Frantsen, J. E., "Corrosion aspects for stainless steel surfaces in the brewery, dairy and pharmaceutical sectors." In ***CORROSION 2009***. OnePetro (2009, March).

36. Davis, J. R. (Ed.)., "Alloy digest sourcebook: stainless steels." ***ASM international*** (2000).

37. Newson, T., "Stainless steel-applications, grades and human exposure." ***AvestaPolarit Oyj Abp*** (2001).

38. Talha, M., Behera, C. K., & Sinha, O. P., "A review on nickel-free nitrogen containing austenitic stainless steels for biomedical applications." ***Materials Science and Engineering****: C*, *33*(7), 3563-3575 (2013).

39. Sheet, S., "Alloy 316/316L." ***An Austenitic Stainless Steel Containing Molybdenum Which is More Corrosion Resistant than the Conventional***, *304* (2014).

40. Solomon, N., & SOLOMON, I., "Phase transformation influence on corrosion resistance of AISI 316 austenitic stainless steel." ***UPB Sci Bull***, *72*, 197-207 (2010).

41. Jagarinec, D., Kirbiš, P., Predan, J., Vuherer, T., & Gubeljak, N., "Analysis of deformation induced martensite in AISI 316L stainless steel." ***Materials Testing***, *58*(6), 547-552 (2016).

42. Nied, H., "The finite element modeling of the resistance spot welding process." ***Weld. J.***, *63*(4), 123 (1984).

43. Peasura, P., “Experiment design with full factorial in gas tungsten arc welding parameters on aluminium alloy 5083.” In ***Advanced Materials Research*** (Vol. 711, pp. 183-187). Trans Tech Publications Ltd (2013).

44. Pires, J. N., Loureiro, A., Godinho, T., Ferreira, P., Fernando, B., & Morgado, J., “Welding robots.” ***IEEE robotics & automation magazine***, *10*(2), 45-55 (2003).

45. Almeida, F. A., Gomes, G. F., Sabioni, R. C., Gomes, J. H. F., Paula, V. R., Paiva, A. P., & Costa, S. C., “A gage study applied in shear test to identify variation causes from a resistance spot welding measurement system.” ***Journal of Mechanical Engineering,*** *64*(10), 621-631 (2018).

46. El-Banna, M., “Dynamic resistance based intelligent resistance welding.” ***Wayne State University*** (2006).

47. Eftekharimilani, P., Van der Aa, E. M., Hermans, M. J. M., & Richardson, I. M., “Microstructural characterisation of double pulse resistance spot welded advanced high strength steel.” ***Science and Technology of Welding and Joining***, *22*(7), 545-554 (2017).

48. Zhang, H., & Senkara, J., “Resistance welding: fundamentals and applications.” ***CRC press*** (2011).

49. Pouranvari, M., Asgari, H. R., Mosavizadch, S. M., Marashi, P. H., & Goodarzi, M., “Effect of weld nugget size on overload failure mode of resistance spot welds.” ***Science and Technology of Welding and Joining***, *12*(3), 217-225 (2007).

50. Hu, J., Marciniak, Z., & Duncan, J. (Eds.), “Mechanics of sheet metal forming.” ***Elsevier*** (2002).

RESUME

Mohamed Balaid A Rmadan, graduated from primary and secondary education in this city. He completed high school education in Algaeabulli High School, after that, he started undergraduate program in Almergib University Department of Mechanical Engineering in 2007. Then in 2013, he started assignment as a Research Assistant in Almergib University Department of Mechanical Engineering. Then in 2019, he moved to study a Master Degree in Mechanical Engineering at Karabuk University until now.